Journal of Materials Chemistry B

ROYAL SOCIETY OF CHEMISTRY

PAPER

View Article Online
View Journal

Cite this: DOI: 10.1039/d5tb00137d

A synthetic biomolecular condensate from plant proteins with controlled colloidal properties†

Pratyusha Ghosh,[a] Nataliia Buhaichuk,[ab] Jenna Carr,[a] Sakurako Tani,[c] Raj Shankar Hazra,[d] Sijo Mathew,[e] Yongki Choi[cf] and Mohiuddin Quadir[*af]

Received 20th January 2025,
Accepted 14th June 2025

DOI: 10.1039/d5tb00137d

rsc.li/materials-b

A synthetic biomolecular condensate (sBC) consisting of a prolamin-rich, plant protein, zein, has been engineered. These artificial condensates were prepared from the liquid–liquid phase (LLP) separation of a protein-rich liquid phase in water. To ensure the colloidal stability of the separated condensate, the protein was chemically modified either *via* quaternization with glycidyl trimethyl ammonium chloride (GTMAC) or covalently connecting poly(ethylene glycol) by reductive amination, respectively. The modified protein condensates, termed QZs and PZs (for quaternized and PEG-conjugated zein, respectively) exhibited hydrodynamic diameters (D_H) ranging from 100–300 nm and surface charge or ζ-potential of +35 to −19 mV, which ensured condensate stability *via* inter-particle repulsion. The size, charge, stability, and morphology of the condensate particles can be optimized by mixing both types of modified proteins (QZs and PZs) at a pre-determined stoichiometry. Such stoichiometric interactions of proteins electrostatically and thermodynamically stabilized the sBCs. These sBCs can be enriched with small molecules, which can be exchanged with their bulk environment, showcasing their potential to compartmentalize chemical species. *In vitro* studies indicated cellular internalization and accumulation of sBCs depending on their surface properties. Inspired by the condensation of proteins occurring in cells *via* LLP, this work provides a robust, scalable strategy to design stable, functional condensates that can be used as a platform to understand the structure and function of natural condensates.

1. Introduction

Biomolecular condensates (BCs) are membrane-less assemblies of proteins and nucleic acids and are well-established cellular entities which can selectively compartmentalize compounds and chemical processes vital for cellular organizations.[1] Formed *via* liquid–liquid phase separation (LLPS) of protein-rich phases in an aqueous environment of the cells, BCs come in a wide range of sizes.[2] The nucleolus and stress granules are primordial examples of large BCs and have been extensively studied *in vitro*. BCs, particularly under *in vivo* conditions, are within the nanoscale range, <100–300 nm in diameter containing multiple copies of the constituent molecules.[3] With the progress of our understanding of cellular biology, BCs are gaining increasing traction because of their roles in cellular homeostasis and pathology.[4] Ranging from amyloid plaque formation in neurodegenerative diseases[5] to aging,[6] and cancer,[7] BCs have been implicated in disease initiation, maintenance, and proliferation. As such, therapeutic interventions targeted to disrupt the form and function of disease-associated BCs have spurred the emergence of several translational molecules. This has become increasingly important to study the mechanism of formation, action, and size-function relationship of BCs, particularly those composed of proteins, in the context of their *in vitro* and *in vivo* implications in health and diseases. Synthetic biomolecular condensates (sBCs) are ideal platforms to investigate the compositional and structural attributes of natural condensates, *in vitro*, and to connect with their functional role, such as compartmentalization and condensation of target compounds.[8] Synthetic polypeptides are an attractive chemical platform to prepare artificial BCs.[9] The presence of multiple functional groups, pre-defined secondary conformations, and the possibility to include stimuli-responsive – particularly thermo-sensitive – residues within the peptide backbone are important features of synthetic polypeptides for their applications for developing sBCs.[10] We aimed

[a] *Department of Coatings and Polymeric Materials, North Dakota State University, Fargo, ND 58102, USA. E-mail: mohiuddin.quadir@ndsu.edu; Tel: + 1701-231-6283*
[b] *Lviv Polytechnic National University, Lviv 79013, Ukraine*
[c] *Department of Physics, North Dakota State University, Fargo, ND 58102, USA*
[d] *Department of Mechanical Engineering, North Dakota State University, Fargo, ND 58102, USA*
[e] *Department of Pharmaceutical Sciences, School of Pharmacy, North Dakota State University, Fargo, ND 58102, USA*
[f] *Materials and Nanotechnology Program, North Dakota State University, Fargo, ND 58102, USA*

† Electronic supplementary information (ESI) available. See DOI: https://doi.org/10.1039/d5tb00137d

to develop sBCs using chemically modified plant proteins, such as zein. A prolamin protein derived from maize (*Zea mays*) endosperm, zein is the main storage protein of the plant, constituting almost 50% of the corn proteins.[11] The protein was certified as a Generally Recognized As Safe (GRAS) material in 1985 by the Food and Drug Administration (FDA) and has been used in multifarious commercial colloidal preparations.[11–16]

To our advantage in designing sBCs, zein proteins showcase interesting colloidal properties, which are key attributes of natural biomolecular condensates. The origin of these properties is rooted in the capacity of the protein to self-assemble. Various self-assembly techniques have been adopted to prepare colloidal particles of zein, including emulsification, solvent evaporation, phase separation,[12] solvent precipitation,[13] anti-solvent dialysis, pH driven nanoprecipitation,[14,15] and electrohydrodynamic atomization.[16] The critical challenge of using zein as a representative platform to study condensates is the fundamental colloidal instability of the protein. Colloidal stability is defined by various particle-related properties including aggregation, core composition, shape, size, and surface chemistry.[17] The inherent tendency of zein colloidal suspensions to aggregate and precipitate at near-neutral pH or under high ionic strength conditions is primarily due to reduced electrostatic repulsion and enhanced hydrophobic interactions.[18] In aqueous dispersion the hydrophobic interactions dominate in particle coalescence and loss of colloidal stability. Colloidal structures, as those of condensates, are generally unstable due to high surface energy, leading to high reactivity. To gain stabilization of a colloidal dispersion it can be achieved through three primary mechanisms: electrostatic, steric, and electrosteric stabilization.[19] Electrostatic stabilization relies on surface charges that create repulsive forces between particles, preventing their aggregation.[20–23] Steric stabilization, on the other hand, uses adsorbed macromolecules or surfactants that form a protective layer around the condensates, providing spatial separation among them.[21,24] In many cases, a combination of both electrostatic and steric mechanisms is required to stabilize colloidal systems from various destabilization forces.[15,25–27] To improve colloidal stability of zein proteins, stabilizers such as sodium caseinate and various surfactants like Tween 20 and Pluronic F86 are widely used.[28,29] Sodium caseinate, for instance, provides steric and electrostatic stabilization by adsorbing onto the surface of zein-derived sBCs, forming a protective layer that prevents aggregation.[29,30] Similarly, surfactants like polysorbates (*e.g.*, Tween 80), or Pluronic F68, enhance dispersion of colloidal particles by reducing surface tension and providing steric hindrance.[31,32] Another approach for augmenting the colloidal stability is to adjust the pH of the particle suspension. The isoelectric point of zein is around pH 6.2, and lowering the pH to 4–5 protonates the amino groups, creating strong charge repulsion between particles. This prevents aggregation and improves the redispersibility of the colloidal particles of zein.[28] Due to such limiting hydrophobic nature of the protein, zein is not amenable to LLPS to produce a uniform and colloidally stable platform for a longer time scale. Furthermore, the inclusion of these synthetic materials to stabilize sBCs produced from zein will further disconnect the platform from recapitulative *in vivo* conditions. Therefore, we adopted a new chemical modification strategy to render the protein amenable to LLPS, thereby favoring the formation of sBCs. Our approach included the incorporation of a positively charged, *i.e.*, quaternized amine residue within the primary structure of the protein, which will favor the formation of sBCs *via* LLPS, and will ensure particle stability *via* an electrostatic mechanism provided by the cationic surface charge. This approach was achieved *via* reacting zein with glycidyl trimethylammonium chloride (GTMAC) under basic conditions, to produce quaternized zein protein (QZ proteins).[33,34] In the second approach, we incorporated a hydrophilic polymer segment at the N-terminal of the protein. This was achieved by connecting an aldehyde-terminated poly(ethylene glycol) to the N-terminal residue of the protein *via* a Michael addition-type reductive amination reaction to produce PEG-modified zein (PZ proteins). The objective of these modifications is to promote the formation of sterically stabilized sBCs *via* LLPS of an otherwise hydrophobic protein that is prone to uncontrolled aggregation. *Via* adopting a liquid-based phase separation technique, and by promoting interactions between the native protein with a specified amount of the modified, *i.e.*, QZ or PZ proteins, we were able to form distinct sBCs with a narrow size distribution (in terms of hydrodynamic diameter, D_H), controllable surface charge (in terms of ζ-potential), distinct morphology (identified *via* TEM and AFM) and augmented colloidal stability. With a particular emphasis on how composition affects BC formation and structure, we anticipate that the chemically modified zein protein colloids as models of sBCs will provide a new cell-free, straight-forward platform to study the size–surface–function relationship of protein condensates in the context of molecular compartmentalization.

2. Materials and methods

2.1. Materials

Zein protein from maize was purchased from Tokyo Chemical Industries (TCI) (Tokyo, Japan). Methyl poly(ethylene glycol) aldehyde (mPEG-aldehyde) of molecular weight 5 kDa was purchased from Creative PEGWorks (Chapel Hill, NC, USA). Sodium cyanoborohydride ($NaCNBH_3$), glycidyl trimethylammonium chloride (GTMAC) (technical $\geq$90%), sodium hydroxide (NaOH), hydrochloric acid (HCl 37% v/v), di-sodium hydrogen phosphate dihydrate ($Na_2HPO_4{\cdot}2H_2O$), sodium dihydrogen phosphate monohydrate ($NaH_2PO_4{\cdot}H_2O$) sodium chloride (NaCl), ethyl alcohol (anhydrous $\geq$99.5%) and pyrene was purchased from Sigma-Aldrich (St. Louis, Missouri, USA). Dimethyl sulfoxide-D_6 ($>$99.8%) and ninhydrin were purchased from Oakwood Chemicals (Estill, South Carolina, USA). Doxorubicin hydrochloride was purchased from LC laboratories. Regenerated cellulose (RC) Dialysis Tubing (average flat width 32 mm) with a molecular weight cutoff (MWCO) of 3.5–5.0 kDa or 6–8 kDa was purchased from Repligen (SpectraPor®, Waltham, Massachusetts, USA). For fluorescence

tagging Alexa fluor 647 NHS ester, Alexa fluor 488 phalloidin, NucBlue™ Fixed Cell ReadyProbes™ Reagent (DAPI), were procured from Thermo Fisher Scientific Inc. (Waltham, Massachusetts, USA). Dulbecco's phosphate buffered saline and DPBS (with $MgCl_2$ and $CaCl_2$, liquid, sterile-filtered, suitable for cell culture) were procured from Sigma-Aldrich and DMEM 1× (Dulbecco's modified Eagle's medium with 4.5 g L^{-1} glucose, L-glutamine, sodium pyruvate) was purchased from Thermo Fisher Scientific Inc (Waltham, MA, USA). 10× Tris/SDS/glycine running buffer, 4× Laemmli sample buffer, 4–20% mini-PROTEIN®TGX™ Precast Protein Gels, 10-well, 50 μL, Precision Plus Protein Dual color standards 500 μL was purchased from Bio-Rad (Hercules, California). β-Mercaptoethanol, methanol, FITC and glacial acetic acid were purchased from Thermo Fisher Scientific Inc. (Waltham, Massachusetts, USA).

2.2. Quaternization of zein – synthesis of QZ proteins

The quaternization of zein was achieved by reacting the commercially procured zein with glycidyl trimethyl ammonium chloride (GTMAC), a quaternary ammonium compound (Scheme 1A), following modification of published procedures.[34,35] In this method, zein protein (500 mg) was dissolved in 8 mL of 60% (v/v) ethanol solution. Subsequently, 2 mL of GTMAC (density1.13 g mL^{-1} at 20 °C) was introduced to the protein solution drop-wise under continuous stirring with a bar magnet. The pH of the reaction mixture was adjusted to pH 10 using a 4 M sodium hydroxide (NaOH) solution. The reaction was continued for 1 h at 60 °C and terminated by reducing the pH of the suspension to 7.0 by adding a 4 M HCl solution. No precipitation was observed after this neutralization. Therefore, the reaction product was purified *via* dialyzing the reaction mixture using RC membranes of MWCO 3.5 kD against water for 18 h to get the product of quaternized zein (QZ).[34,35]

2.3. Hydrophilic modification of zein by PEG-conjugation

The conjugation of mPEG-aldehyde to the ε-amino groups of lysine residues in zein was performed *via* Michael's addition type reductive amination reaction (Scheme 1B).[36] The reaction was conducted in a conjugation buffer composed of 0.1 M sodium phosphate and 0.15 M sodium chloride, the pH of which was adjusted to 7.4. First, 20 mg of mPEG-aldehyde solution in a freshly prepared conjugation buffer (1 mL) was prepared so that the mPEG-aldehyde concentration of the stock solution is 20 mg mL^{-1}. Zein (10 mg) was dissolved in a solvent system (1 mL) that is composed of 60% (v/v) ethanol and 40% (v/v) conjugation buffer prepared as above. Subsequently, 1 mL of the protein solution was added to 1 mL of mPEG-aldehyde solution slowly under continuous stirring at 300 rpm with the help of a bar magnet. After 15 min of mixing, 10 mg of $NaCNBH_3$ was added as a reducing agent.[37] The pH of the reaction mixture was adjusted to 4–5 using 1 N HCl. The reaction was allowed to proceed for 3 h at room temperature under continuous stirring. After the stipulated time, the clear solution was directly transferred to a dialysis chamber (MWCO = 6–8 kDa), and the product was dialyzed against water to obtain PEG conjugated-zein (PZ). Both the QZ and PZ proteins were characterized with FTIR, ^{1}H NMR, ninhydrin assay, circular dichroism (CD), and *via* elemental analysis as described below.

2.4. Fourier transform infrared spectroscopic (FTIR) analysis

FTIR spectroscopic measurements were conducted using a Thermo Scientific Nicolet 8700 spectrometer. Samples were applied onto potassium bromide (KBr) pellets for analysis. Transmittance spectra were acquired in the mid-infrared region, spanning 4000–500 cm^{-1}, with a spectral resolution of 4 cm^{-1} with 32 scans.

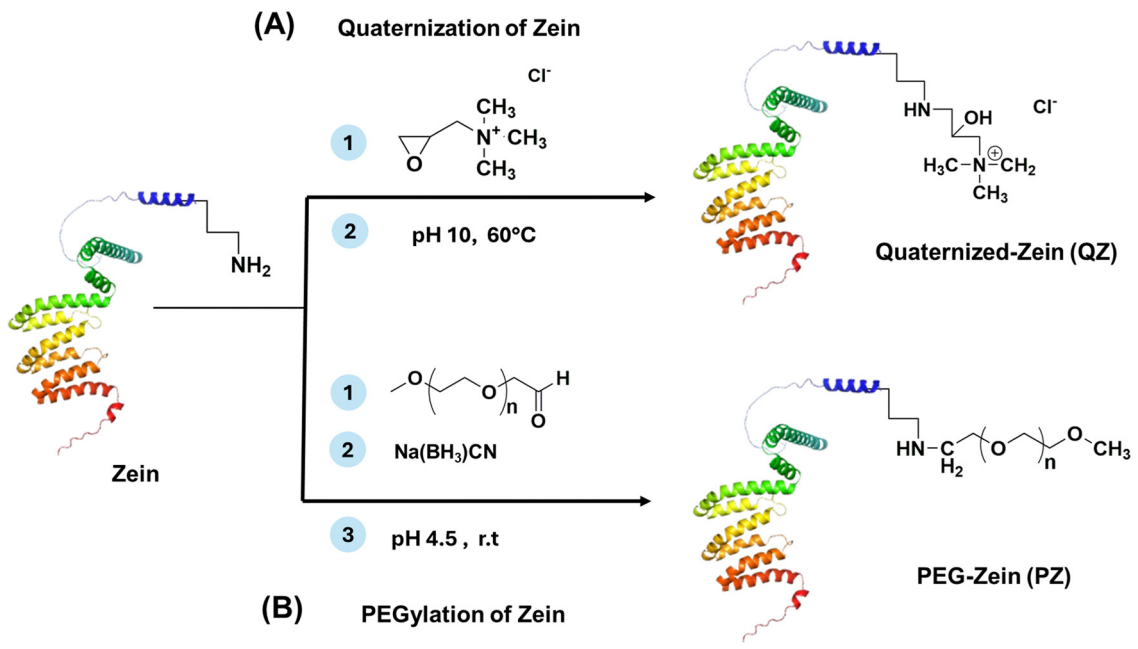

Scheme 1 Reaction scheme for modification of zein: (A) quaternization of zein with GTMAC; (B) conjugation of PEG with zein *via* reductive amination.

2.5. Determination of the degree of functionalization of modified proteins

The degree of functionalization of zein upon reaction with either GTMAC or mPEG-aldehyde was determined using a ninhydrin colorimetric assay, comparing the starting material (native zein) as the control following the published procedure.[38] In this method, QZ (2 mg) or PZ (2 mg) were separately dissolved in DMSO (2 mL, Fischer Chemicals) to prepare a 1 mg mL^{-1} stock solution of the modified proteins in DMSO. A freshly prepared 10 mL ninhydrin solution in ethanol was prepared by dissolving 200 mg of ninhydrin in 10 mL of 99% ethanol. The ninhydrin solution (150 μL) was added dropwise to 2 mL of the protein solution. The mixtures were then incubated in a water bath at 85 °C until a faint orange color was developed. As zein is a protein of the prolamin family it developed this faint orange color instead of the characteristic Ruhemann's purple color that originated upon the reaction of a primary amine with ninhydrin.[38] The absorbances of the samples were measured using a UV-Vis spectrophotometer at an absorption maximum (λ_{max}) of 600 nm. The degree of functionalization was calculated using the following equation.

$$\text{mg of } \alpha\text{-amino acid} = \frac{\text{Abs test} - \text{Abs blank}}{\text{Abs standard} - \text{Abs blank}} \quad (1)$$

2.6. Circular dichroism (CD) spectroscopy of the modified proteins

The CD experiment was carried out using a JASCO J-815 spectrometer in a 0.1 cm path-length quartz cuvette. The baseline was adjusted using 60% ethanol as all the products were completely soluble in this solution. The spectra of all samples were recorded at 25 °C by averaging three scans acquired from 260 to 176 nm (1 nm bandwidth) in 0.2 nm steps at a scanning rate of 50 nm min^{-1}.[39]

2.7. X-ray photon spectroscopy (XPS)

XPS was performed using Thermo electron K-Alpha™ X-ray photoelectron spectroscopy (XPS). Samples were mounted on carbon tape and loaded into the XPS and pumped down to 10^{-6} mTorr before the experiment. The survey scans were run at 200 eV with a dwell time of 10 milliseconds, and an energy step size of 1 eV.

2.8. Thermogravimetric analysis (TGA) of proteins

For determining the thermal degradation and decomposition behavior of QZ and PZ proteins in comparison to unmodified proteins, thermogravimetric analysis was conducted using a Q500 thermogravimetric analysis (TGA) system (TA Instruments) with a heating ramp rate of 10 °C min^{-1} from room temperature to 700 °C.

2.9. Gel electrophoresis of zein and modified zein

To evaluate the molecular weight distribution, and assess potential modifications of zein and its derivatives, sodium dodecyl sulfate-polyacrylamide gel electrophoresis SDS-PAGE was performed under denaturing conditions. Native zein, PZ, and QZ were dissolved separately in 60% (v/v) ethanol and 40% 1× Tris/SDS/glycine running buffer (Bio-Rad). The final concentration of the proteins in the solution was 1 mg mL^{-1}. For each sample, 5 μL of the protein solution was mixed with 25 μL of running buffer and 10 μL of Laemmli sample buffer containing β-mercaptoethanol as a reducing agent (β-mercaptoethanol: 4× Laemmli buffer prepared in a 1 : 9 ratio). The mixtures were heated at 95 °C in a water bath for 5 minutes to ensure complete protein denaturation and reduction of disulfide bonds. A 5 μL aliquot of protein ladder was loaded into the first well of a precast SDS-polyacrylamide gel purchased from BioRad. Subsequently, 40 μL of the protein samples (zein, PZ, or QZ) were loaded into separate wells. Electrophoresis was conducted initially at a constant voltage of 60 V for 1 h to allow sample stacking, followed by 100 V for an additional 1 h to achieve protein separation based on molecular weight. Upon completion of the electrophoresis, the gel was stained using Coomassie Brilliant Blue staining solution prepared with 200 mg Coomassie Brilliant Blue R-250 dissolved in 50 mL methanol, 10 mL glacial acetic acid, and 40 mL deionized water. The gel was incubated in the staining solution for 2 h with gentle agitation. Excess stain was removed by immersing the gel in a destaining solution (methanol : acetic acid : water, 5 : 1 : 4 v/v/v) overnight until a clear background was achieved. Later the gel image was taken by an Azure-200 gel imager with an orange background.

2.10. Preparation of sBCs by self-assembling QZ and PZ with the native protein

The formation of sBCs composed of QZ or PZ and native zein was achieved by an LLPS method, popularly known as non-solvent induced phase separation (NIPS). This process demonstrated in Fig. 1 involves dissolving a specific ratio of the modified proteins, *i.e.* QZ or PZ and the native, unmodified zein protein in a water-miscible compatible solvent. The resulting solution is then added to an aqueous phase, which serves as a non-solvent for the protein. As the water miscible solvent diffuses into the aqueous phase, the protein becomes insoluble and precipitates in the form of condensates at nanoscale dimensions.[40] In our case, five (05) different sBCs composed of QZ or PZ and zein mixed in different weight ratios were prepared using 60% ethanol in water (v/v) as a solute-compatible solvent and deionized (DI) water as the solute-precipitating solvent. More specifically, first, different amounts of QZ or PZ and native zein, according to Table 1, were added to 1 mL of 60% ethanol in water to obtain the targeted % wt/volume of protein in the solvent. This solution is added in a drop-by-drop pattern in the non-solvent (water) under continuous stirring at 100 rpm. The addition was completed in 10 min, and the stirring was continued for 4 h which resulted in the formation of sBCs. The compositions of the formed sBCs (based on the feed ratio of QZ, PZ, or unmodified protein) are presented in Table 1. To remove ethanol and promote the formation of the sBCs of relatively uniform distribution, the protein suspension was dialyzed against water using an

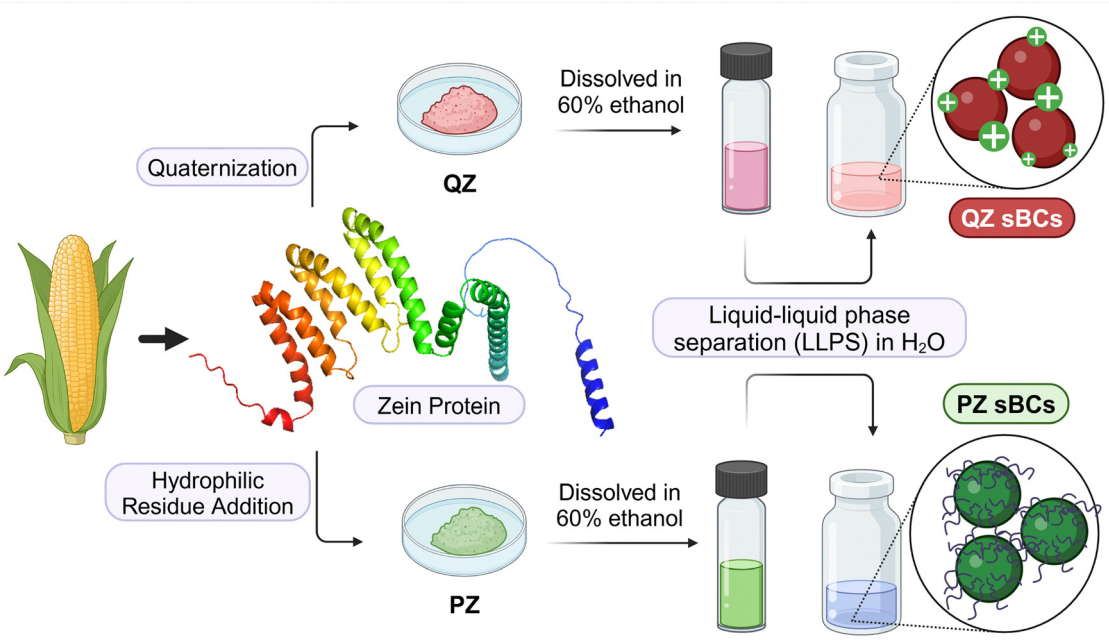

Fig. 1 Fabrication of sBCs of zein with QZ or PZ by a liquid–liquid phase separation (LLPS) method. 60% ethanol was used as a solvent where DI water was used as nonsolvent. The sBC suspensions were purified by dialysis against DI water.

Table 1 Formulations used for making mixed QZ and PZ sBCs with zein[a]

	Zein (mg)	QZ (mg)		Zein (mg)	PZ (mg)
Z100	10	—	Z100	10	—
QZ30	7	3	PZ30	7	3
QZ50	5	5	PZ50	5	5
QZ70	3	7	PZ70	3	7
QZ100	—	10	PZ100	—	10

[a] QZ and PZ proteins are mixed with the unmodified protein in a total volume of 1 mL of 60% ethanol and added in 2 mL of DI water to promote LLPS leading to the formation of sBCs.

RC membrane of MWCO of 3.0–3.5 kDa. As a control, sBCs composed of zein protein entirely (no incorporation of QZ or PZ variants), are referred to as Z100, while those mixed with QZ or PZ systems, are referred to as QZ or PZ followed by the percentage of these modified proteins in the sBCs. Condensates composed of QZ or PZ proteins are referred to as QZ 100 or PZ 100.[39,41]

2.11. Synthesis of fluorescently labeled QZ and PZ proteins

The fluorescent dye, Alexa Fluor™ 647 NHS Ester (Succinimidyl Ester), was dissolved in DMSO to a stock concentration of 0.2 mg mL^{-1}. In a 1.5 mL aliquot of the preformed sBC suspension, 20 μL of the dye stock solution was slowly added while gently mixing using a magnetic stir bar. The reaction mixture was incubated at room temperature for 1 h, and protected from light by wrapping the container in aluminum foil for conjugating the sBCs with the fluorescent dye. The dye-conjugated sBCs were then dialyzed against PBS for 8 h using a dialysis membrane with an MWCO of 6–8 kDa for purification purposes. Following dialysis, protein concentrations were determined *via* bicinchoninic acid assay (BCA assay).

2.12. Evaluation of nanoscale features, *i.e.*, colloidal size, distribution and surface charge of sBCs

The colloidal size of sBCs in terms of D_H and distribution in terms of polydispersity indices (PDI) of the prepared sBCs were evaluated *via* dynamic light scattering (DLS) using disposable polystyrene cuvettes (1 mL, Malvern Panalytical). The surface charge, *i.e.*, ζ-potential of sBCs was measured by utilizing the electrophoretic mobility of the colloidal particles under an applied electric field, as determined by laser Doppler electrophoresis. To ensure statistical reliability, all measurements were conducted in triplicate ($N = 3$).

2.13. Transmission electron microscopy

The microstructural analysis of the sBCs was conducted using high-resolution transmission electron microscopy (HR-TEM). Micrographs were acquired with a JEOL JEM-2100 LaB6 instrument (JEOL USA, Peabody, MA), operating at an accelerating voltage of 200 kV.

2.14. Atomic force microscopy (AFM)

AFM analysis of sBCs, including PZ70 and QZ70, was conducted to evaluate their size and nanomechanical properties. Samples were prepared by incubating 20 μL of sBC solution on silicon substrates (University Wafer) for 10 minutes in a sealed compartment at room temperature to minimize evaporation. After incubation, excess water was gently removed, ensuring that sufficient surface moisture remained to preserve the hydrated state of the condensates during measurement. Imaging and spectroscopy were performed under ambient conditions using an NT-MDT NTEGRA AFM system equipped with V-shaped silicon nitride probes (spring constant: 0.08 N m^{-1}, tip face

angle: 35°). The spring constant was calibrated *via* thermal noise fluctuation, and deflection sensitivity was calibrated using force-indentation on bare silicon wafers. Randomly selected sBCs were imaged at a resolution of 256 × 256 pixels with scan rates of 0.1–0.5 Hz, adjusted based on scan area and particle size. Images were flattened to remove background noise and tilt. Relative stiffness (Young's modulus) was extracted from force-indentation curves using the Hertz model with a shallow indentation depth of 10% of particle size to minimize substrate effects.[42,43] Surface roughness was analyzed using Image Analysis P9 software, calculating the root-mean-square roughness (R_{rms}) from five areas (80 × 80 nm^2) in the central region of each sample.[44]

2.15. Thermodynamic stability measurement of sBCs

The critical aggregation concentrations (CACs) of the sBCs, formed from the self-assembly of zein with PZ or QZ, were determined utilizing fluorescence spectroscopy using pyrene as a hydrophobic fluorescent probe, following an established protocol.[45] A stock solution of pyrene (0.1 mM) was first prepared in dichloromethane. Aliquots (10 μL) of this solution were dispensed into a series of vials, and the solvent was allowed to evaporate *via* overnight air-drying at room temperature. Subsequently, 1.0 mL of varying concentrations of sBCs (ranging from 0.001 to 1000 μg mL^{-1}, 1 mL) were introduced to each vial, maintaining a final pyrene concentration of 1 μM for all samples. The mixtures were subjected to sonication for 90 min, followed by an equilibration period of 3 h at room temperature prior to spectroscopic analysis. Fluorescence emission spectra were acquired using a Jobin Yvon Fluorimeter Fluoromax-3 with an excitation wavelength of 337 nm, with both excitation and emission slit widths set at 2.5 nm. The intensity ratio of 373 nm to 384 nm signals of pyrene was plotted as a function of sBC concentration. The CAC was determined from the inflection point of the resulting curve, in accordance with established methodologies.[45]

2.16. Enrichment of a guest molecule inside protein sBCs

We evaluated the capacity of the sBCs to condense or compartmentalize small molecules using doxorubicin (DOX, MW = 543.5 g mol^{-1}, pK_a = 8.01) as a model compound. The reason for using this compound as the molecular surrogate is the ease of detection and pH-dependent protonation. We selected QZ 70 as a model or representative sBCs, which is composed of 70% quaternized and 30% unmodified zein, for enrichment with DOX. A solution containing 20 mg of QZ70 suspension (as preformed sBC) and 20 mg of PZ70 suspension (also as preformed sBC) with 10 mg of DOX in each vial was dissolved in 2 mL of 60% (v/v) ethanol. This solution was introduced dropwise into 4 mL PBS under continuous magnetic stirring, facilitating the formation of DOX-condensed sBCs. The exact same protocol was used to prepare sBCs of PZ70 enriched with DOX. The resulting dispersion was maintained under stirring for 2 h at room temperature to ensure complete compartmentalization or association of DOX with the sBCs. Subsequently, the sBC suspension was purified *via* dialysis against 1000 mL of PBS using a dialysis membrane with an MWCO of 6–8 kDa. The dialysis medium was regularly replaced until no further diffusion of DOX in the bulk media was visually detectable, indicating the removal of sBC-free DOX. To quantify the efficiency of uptake, and loading content of DOX inside sBCs, the dialyzed sample was freeze-dried. Later 1 mL of ethanol was added to the dried DOX-associated sBCs in order to solubilize and disrupt the particle structure and induce complete DOX dissociation from sBCs. The ethanol was allowed to evaporate under room temperature and pressure. A predetermined amount of PBS was added to the sample and sonicated so that DOX was completely dissolved in the media. The sample was redispersed and filtered *via* a centrifugation filter at 10 000 rpm (MWCO = 3 kDa, VWR International LLC USA). The filtrate solution was quantified to determine the amount of DOX that was compartmentalized within the sBCs using UV-Vis spectroscopy at λ_{max} for DOX at 480 nm. The DOX compartmentalization efficiency of sBCs was calculated using eqn (2), and the loading content of DOX within sBCs was calculated using eqn (3) as presented below.[41,46]

$$\text{DOX compartmentalization efficiency } \% = \frac{\text{DOX amount loaded in sBCs}}{\text{Initial feed of DOX}} \times 100 \quad (2)$$

$$\text{DOX content } \% = \frac{\text{DOX amount entrapped in sBCs}}{\text{Total weight of sBCs}} \times 100 \quad (3)$$

2.17. Dissociation kinetics of the guest molecule as a function of time and pH

The dissociation kinetics of DOX from sBCs were evaluated by monitoring the absorbance of the free DOX at 480 nm over 33 hours at 25 °C. A predetermined amount of DOX-loaded sBC suspensions was introduced in a dialysis bag (Repligen®, MWCO 6–8 kDa) and completely submerged in either PBS (pH 7.4) or pH 5.5 phosphate buffer (pH adjusted with strong acid) in a 250 mL beaker. The samples were continuously agitated by an orbital shaker (Heathrow Scientific, Vernon Hills, Il, USA) at 65 rpm. After a predetermined time interval, 3 mL of sample buffer was collected from the bulk media (outside the dialysis membrane) and replenished immediately with the same volume of buffer media maintained at a similar temperature. The experiment was continued for 33 h and the amount of DOX in the sample was measured using UV-Vis spectroscopy (Varian Cary 5000, Santa Clara, CA, USA). Based on the intensity of the absorption peak at 480 nm, the DOX concentration of the withdrawn media, *i.e.*, the amount of DOX dissociated from sBCs was determined.[47,48] As a control, an equivalent amount of DOX was dissolved in PBS buffer and their dissociation kinetics was also recorded to examine the diffusion-based release of DOX through the dialysis membrane comparison to that of the sBC-associated DOX. The cumulative

dissociation of DOX over time was calculated by eqn (4).[41,49]

$$\text{Cumuative \% dissociation of DOX} = \frac{\text{Volume withdrawn}}{\text{Volume of bath}} \times \%\ \text{release at time } t + \sum \%\ \text{release at time } t-1 \quad (4)$$

2.18. Effects of sBCs on cell health and cellular uptake

The effect of sBCs on eukaryotic cells was evaluated using an *in vitro* Alamar blue® assay, which determines the proliferation status of the cells in the presence of foreign particles. In our case, sBCs composed of zein only (*i.e.* Z100) were used as a control. Two cell lines, *i.e.*, human embryonic kidney (HEK293) and MIA PaCa-2 pancreatic cancer cells were used as test platforms. For this experiment, 2000 or 4000 cells were seeded in a 96-well plate in DMEM media for 48 h or 24 h studies, respectively. Once the cells reached approximately 70% confluency, the DMEM media was replaced with sBC-spiked media. The cells were then incubated for 24 h before conducting the Alamar Blue assay. Both sBCs of QZ 70 and PZ70 were tested at doses ranging from 1000 μg mL^{-1} to 0.001 μg mL^{-1}. After 24 h of incubation, 20 μL of Alamar Blue® reagent (10% of the well volume) was added to each well and placed in a CO_2 incubator for 4 h (37 °C, 5% CO_2, Thermo Scientific™ Midi CO_2 Incubator, USA). After the incubation period, fluorescence was measured using a SpectraMax Gemini XPS Microplate Reader with an excitation wavelength of 560 nm and an emission wavelength of 590 nm. The cytotoxicity results were analyzed relative to the 100% viability of cells cultured in sBC-free media (control). The same procedure was followed for the 48-h incubation study, where the cells were treated with sBCs for 48 h.

2.19. Confocal microscopic evaluation of cellular uptake of sBCs

Confocal laser scan microscopy was conducted in MICA microhub (Leica Microsystems, Wetzlar, Germany). Both QZ70 and PZ70 dye-labeled sBCs were diluted with DMEM to a final working concentration of 10 μg mL^{-1}. These dye-labeled sBCs were used for confocal microscopy experiments. For this study, MIA PaCa-2 cells were cultured, and 10 000 cells were seeded in glass-bottom ibidi dishes (35 mm). The cells were incubated for 24 h to allow cell adherence and growth. After incubation, the media in the ibidi dishes was replaced with sBC-containing DMEM media. Cells were treated with the sBC suspensions for 24 h at 37 °C. After 24 hours of treatment, the media was removed, and the cells were washed three times with DPBS, and fixed with 4% paraformaldehyde. Subsequently, the cells were incubated in the dark for 20 minutes. Following fixation, cells were gently washed with DPBS. Permeabilization was carried out by treating the cells with 0.1% (w/v) Triton solution for 10 min. Staining of the cell nucleus was performed by adding a DAPI solution (NucBlue™ Fixed Cell Ready Probes™ by Thermo Fisher Scientific) Reagent diluted with DPBS and incubating for 10 minutes.[50] After gently washing with DPBS, the cytoskeleton staining was conducted using Alexa Fluor™ 488 Phalloidin (Thermo Fisher Scientific).[51] After staining, cells were washed with PBS and observed under a bright-field microscope to ensure cell integrity. Dishes were then stored in PBS (2–3 drops to prevent drying) and were observed under confocal microscopy to evaluate sBC localization, nuclear staining, and cytoskeletal organization. A control dish where cells were not treated with dye-labeled sBCs was also prepared.

3. Results and discussion

3.1. Chemical modification of the proteins constituting sBCs

The biomolecules which have been used to form the sBCs were synthesized *via* modification of zein. The synthetic routes to the modified zein proteins, *i.e.*, QZ and PZ, are presented in Schemes 1A and B. The quaternization of zein was successfully achieved by the reaction of the protein with GTMAC under alkaline conditions (pH 10) as shown in Scheme 1A. The reaction was conducted at an elevated temperature of 60 °C.[52] Conjugation of PEG to proteins like zein is an established pathway to modulate the *in vitro* and *in vivo* stability, and hemocompatibility of proteins.[53,54] Chemically conjugating PEG with zein through a carbodiimide reaction has already been reported.[55,56] We opted for a one-step Michael addition to modify the zein protein with PEG due to more orthogonality of reductive amination type reactions. For this reaction, mPEG-aldehyde was conjugated to the L-lysine residue of the protein.[36] Primarily available as α-zein, the zein protein used in this study consists of approximately 0.4–1% lysine residues.[57,58] Thus the PEG conjugation process involves the reaction between the aldehyde group of the PEG, and the ε-amino group of lysine residues in zein to form a Schiff base intermediate. This intermediate is then reduced to create a stable secondary amine linkage in the presence of a reducing agent such as sodium cyanoborohydride $Na(BH_3)CN$ as shown in Scheme 1B.[37]

3.2. Chemical characterization of the sBC-forming proteins by FTIR spectroscopy

The FTIR spectra of the modified proteins, QZ and PZ, which constitute the sBCs, are presented in Fig. 2A. The spectra reveal the characteristic amide I peak for C–N stretching at 1652 cm^{-1} and amide II peaks corresponding to C═O stretching at 1535 cm^{-1}, respectively.[59,60] The presence of these bands suggests that the amide bonds in the protein backbone remain unaltered post-chemical modification. In QZ we can see the appearance of a new peak at 1039 cm^{-1} which corresponds to the C–O stretching of the secondary alcohol originating from the epoxide ring opening of GTMAC.[61] Moreover, a peak at 1096 cm^{-1}, which is most likely due to the C–N bond stretching that formed between GTMAC and the lysine residues in QZ.[62] For the PEG-conjugated zein, PZ, a medium-intensity single peak at 2886 cm^{-1} was formed originating from the symmetric $-CH_2-$ stretching vibrations of long alkyl chains, confirming the presence of PEG in the sample.[63] A distinctive peak at 1103 cm^{-1}, which is characteristic of C–N stretching vibrations

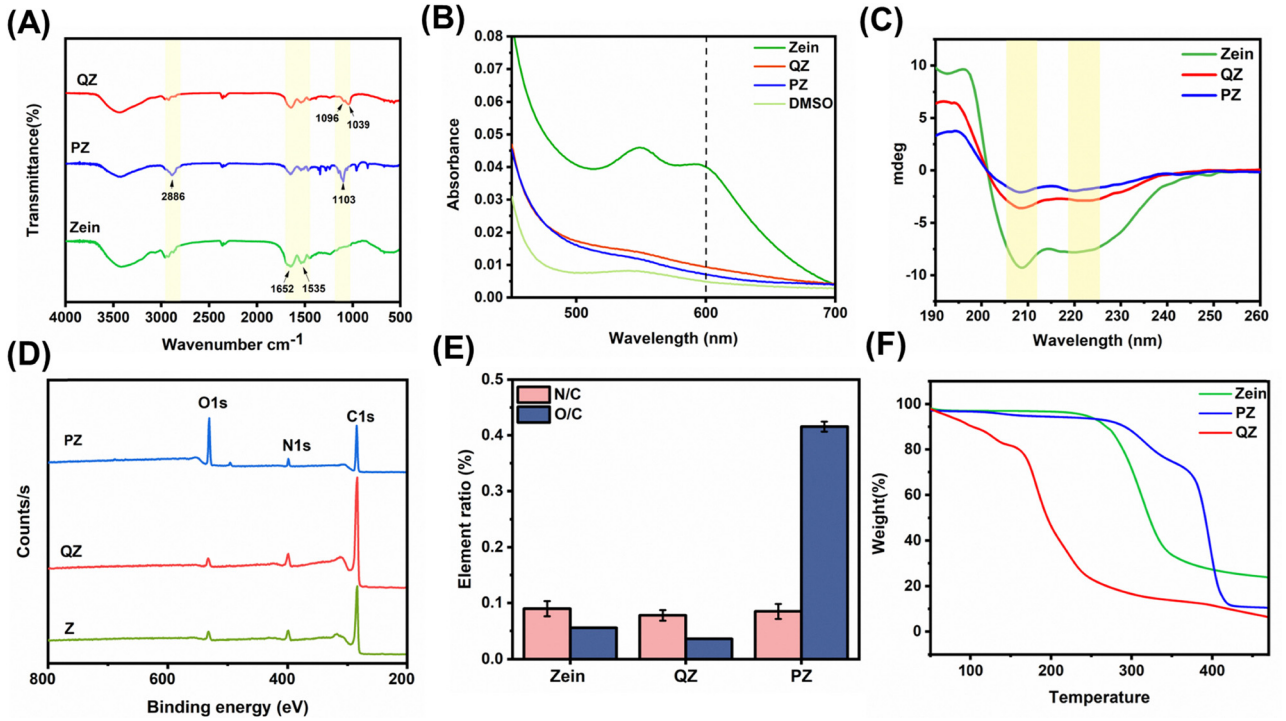

Fig. 2 Chemical characterization of sBC-forming proteins, QZ and PZ using unmodified zein as the control: (A) FTIR spectra of unmodified and modified protein showing the appearance of the new vibration signals at 1096 cm^{-1} and 1039 cm^{-1} for QZ corresponding to the C–N stretching and C–O stretching, respectively. For PZ two new peaks at 2886 cm^{-1} and 1103 cm^{-1} appeared in comparison to zein corresponding to symmetrical $-CH_2-$ stretching and –C–N stretching; (B) ninhydrin assay exhibiting a very distinct peak at 600 nm for zein, which is absent in the spectra obtained of QZ and PZ, indicating a successful conjugation of the GTMAC and PEG respectively to the primary amine containing amino acid residues in zein; (C) circular dichroism (CD) spectra of QZ and PZ exhibiting a reduction of the two characteristic local minima at 208 and 222 nm, most likely due to the reduction of the alpha helical content after the chemical modification of zein; (D) an XPS plot showing the surface elemental composition of QZ and PZ with respect to the unmodified protein; (E) a comparative elemental composition obtained from XPS showing the N/C and O/C ratio in the QZ and PZ systems; (F) a TGA trace of the native zein, QZ and PZ indicating the effect of chemical modifications on the thermal stability of the protein.

of secondary amines appeared in the FTIR spectra of PZ, indicating the successful formation of the PEG conjugate of zein *via* Michael addition (Fig. 2A).

3.3. Determination of the degree of functionalization of the proteins constituting sBCs

The ninhydrin test was adopted to determine the degree of functionalization of the modified proteins, QZ and PZ, which constitute the sBC (Fig. 2B). Zein contains 0.1–4% of lysine residue and is also rich in prolamin. Therefore, we expect that the protein will be sensitive to the ninhydrin test, which is a highly effective assay to quantify the primary (and secondary) amine residues present in amino acids, peptides, proteins, and in other compounds of biochemical relevance.[38] For our case, DMSO was used as the solvent system to trace the degree of modification of zein. Previous studies have shown that the λ_{max} of the ninhydrin reaction product is ~605 nm in nonaqueous aprotic solvents like DMSO or DMF.[64] As presented in Fig. 2B, native zein displays a distinct peak for Ruhemann's purple at 600 nm upon reaction with the ninhydrin reagent, which is absent in the UV-spectra that were obtained for QZ and PZ. This is most likely due to the significant extent of the reaction of zein with GTMAC (for QZ) or mPEG-aldehyde (for PZ). Our results indicated that for QZ and PZ, approximately 86% and 92% of the amino acid residues containing primary or secondary amines have been functionalized by GTMAC and PEG, respectively.

3.4. Evaluation of the secondary structure of the sBC-forming proteins by circular dichroism spectroscopy

Circular dichroism spectroscopy was used to evaluate the conformational changes of the secondary structures of the protein after chemical modifications (Fig. 2C). Earlier studies showed that the peak intensity of zein protein changes with solvent composition, particularly with the ethanol-to-water ratio.[65] Therefore, for our experiment, we used 60% ethanol (v/v) as the solvent for the protein, at a concentration maintained at 100 μg mL^{-1}. We observed that the unmodified zein in this solvent system showed two prominent and intense local minima around 208 nm and 222 nm indicating a very high percentage of α-helical secondary structures within the protein backbone.[66] These CD peaks essentially corresponded to the $\pi \rightarrow \pi^*$ and $n \rightarrow \pi^*$ electronic transitions for the α-helical structure of the protein.[39] This observation is in agreement with the previous studies which showed that zein is rich in α-helical component.[67,68] We further observed that, for QZ,

there is a significant reduction of the α-helical content almost by 56%. On the other hand, for the PZ system, the α-helical content was reduced by approximately 83%. These changes could be due to the disruption of the local hydrogen bonds by the incorporation of GTMAC and PEG moiety within the primary structure of the protein.

3.5. Elemental analysis of the sBC-forming proteins by X-ray photon spectroscopy (XPS)

As expected for PZ, the surface scan using XPS showed a strong presence of elemental oxygen (Fig. 2D) compared to unmodified zein due to the attachment of a 5 kDa PEG to the protein. The XPS spectra of QZ did not exhibit a significant change in N/C ratio (Fig. 2E), mostly due to the presence of a small amount of lysine residues (0.4–1%) within the protein backbone to which the GTMAC residue (M.W. = 151.63 g mol^{-1}) could be conjugated. The elemental analysis revealed the composition of N, C, and O (in %) before and after the modification (Fig. 2E), where the N/C and O/C ratio for QZ and PZ indicated the changes in the elemental composition after the chemical modification validating our observations with the XPS measurement. The nitrogen-to-carbon (N/C) and oxygen-to-carbon (O/C) ratios were calculated from the atomic percentages of each element as obtained from the XPS survey spectra and shown in Fig. 2E. The ratios were calculated as: N/C ratio = (atomic % of N)/(atomic % of C), and for O/C ratio = (atomic % of O)/(atomic % of C).

3.6. Thermal stability of the sBC-forming proteins

The thermal stability properties of zein and the modified zein (QZ and PZ) were estimated by thermal gravimetric analysis (Fig. 2F). This analysis was done to identify the physical stability, the success of chemical modification, and purity of the modified proteins that constituted the sBCs. We observed that the unmodified protein was stable up to 300 °C, with an initial weight loss of 5% that is probably due to water evaporation.[69] A significant mass loss of zein took place around 300 °C, which could be due to the thermal degradation of the protein that is consistent with previous literature reports.[70,71] Interestingly, we observed that the conjugation of PEG to zein increased the thermal stability of the product (PZ) in accordance with earlier studies.[72,73] Practically, this product showed a two-step degradation pattern, where the early stage corresponds to the decomposition of PEG,[74] while the later stages involve the degradation of the zein backbone. For QZ a significant shift and change in thermal stability behavior can be seen from the TGA trace. The first stage of decomposition took place from 25–130 °C. This is most likely originated from the surface-bound moisture associated with the product formed from the reaction of zein with GTMAC under alkaline conditions. The significant mass loss started at around 150 °C, which could be associated with the decomposition of the protein backbone. This result follows the previously studied literature which has shown that the increased amount of GTMAC in the chitosan/PLA composite films showed the lowest thermal stability.[75,76]

3.7. SDS-PAGE gel electrophoresis of zein and modified zein

SDS-PAGE gel electrophoresis was conducted to confirm protein purity and modifications. The major bands appear around 20–25 kDa and a faint signal appears at ∼45 kDa (Fig. 3A). This is consistent with the known molecular weight range of α-zein monomers (∼19–22 kDa) and a minor fraction of β- or γ-zein components (32–45 kDa).[77] Fig. 3A also demonstrates a band appearing at slightly higher molecular weights than unmodified zein (in lane 3), particularly around 25–30 kDa and ∼50 kDa. This is possibly due to the increment of molecular weight of GTMAC-conjugated zein that reduced the protein mobility due to the presence of cationic charge. Fig. 3B shows the gel electrophoretic migration for PZ (lane 3), which shows a similar banding pattern to the native zein, with slight migration and band broadening indicative of successful PEG conjugation. The conservation of the primary band of zein around 22–25 kDa confirms that the protein backbone remains intact after the PEGylation reaction, suggesting that the conjugation process did not lead to fragmentation or degradation of the native protein.

3.8. Nanoscale features of the sBCs

We prepared sBCs using LLPS, where the varying ratio of unmodified zein was mixed with chemically modified proteins (either QZ or PZ). For the LLPS, a 60% v/v ethanol solution in water was used as the conducive solvent to dissolve the mixture of modified and unmodified protein. This protein-rich phase was slowly added to water, to form sBC particles, which were later purified by dialysis against water. The compositional variations of sBCs are presented in Table 1. This strategy is adopted to systemically regulate the nanoscale features of the resulting colloidal particles, such as D_H, ζ-potential, and particle size distribution. The D_H of the sBCs was measured *via* DLS. We also formed sBCs composed of unmodified zein (no QZ or PZ added) for use as controls. We observed that sBCs fabricated from unmodified zein were larger, with a D_H of 173 ± 15 nm and a PDI of 0.9 (Fig. 4A). This indicates a significant extent of aggregation and/or coalescence took place affecting the heterogeneous distribution of the sBC particles. Similar trends have been observed in earlier studies, where colloidal particles prepared with unmodified zein tend to form aggregates due to the inherent hydrophobic nature of the protein.[78] On the other hand, sBCs composed of quaternized zein (*i.e.* QZ 100) exclusively, displayed the lowest D_H of 47 ± 4 nm with a PDI of 0.1. Transmission electron microscopic images of QZ100 are presented in Fig. 5A. Condensates composed of unmodified zein mixed with quaternized zein at 30, 50 or 70 w/w% ratio (*i.e.* sBCs QZ30, QZ50, and QZ70) showed a gradual enhancement of D_H from 64 ± 8 nm, 72 ± 5 and 81 ± 9 nm, respectively as shown in Fig. 4A. Quaternization modifies the surface chemistry of proteins, by incorporating cationic charges, rendering the protein more hydrophilic. Upon LLPS of the protein-rich phase, these charges promote electrostatic repulsion and reduce the propensity of otherwise hydrophobic proteins to aggregate into larger particles. As such, the sBCs composed of

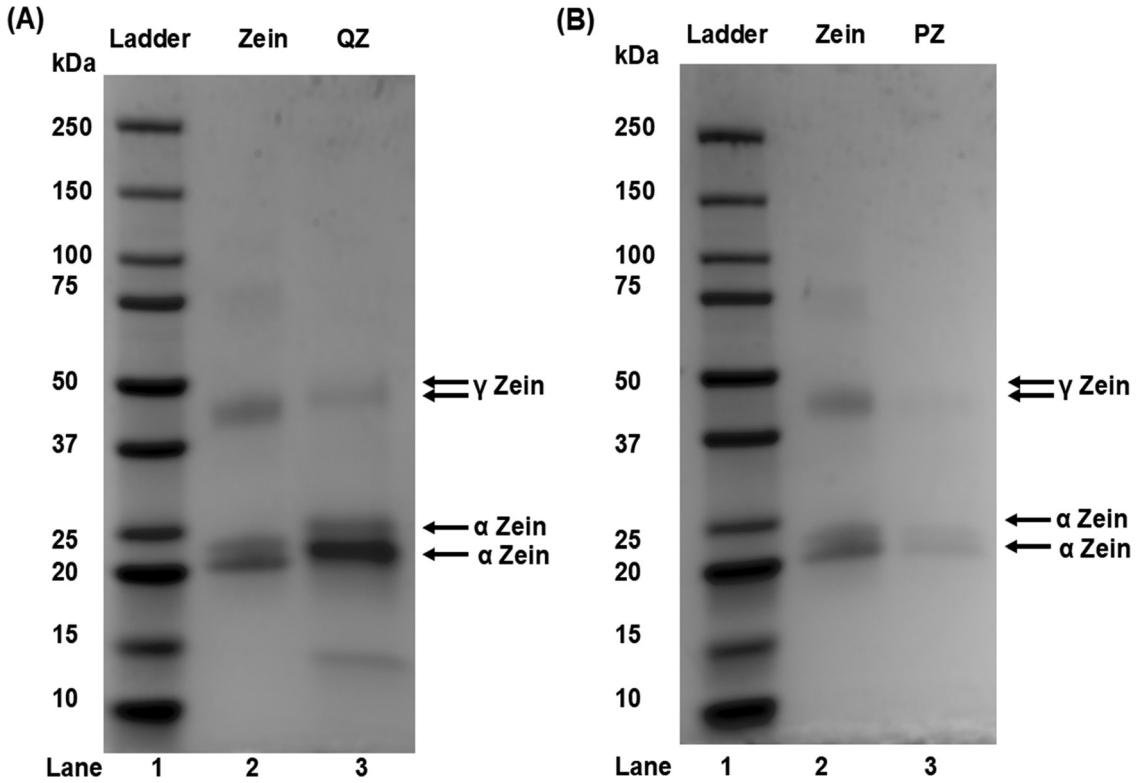

Fig. 3 (A) SDS-PAGE Gel electrophoresis of zein and quaternized zein. (B) SDS-PAGE Gel electrophoresis of zein and PEG–zein.

QZ present smaller D_H, which are less likely to coalesce together into larger aggregates.[79] Notably, sBCs composed of 70% quaternized protein (*i.e.*, QZ70) show the most uniform size distribution with a PDI of 0.06. The variation in the D_H of the sBCs with changing composition is primarily governed by the interplay between colloidal stabilization mechanisms *i.e.*, electrostatic and steric interactions during LLPS, and the inherent properties of unmodified zein. In the case of QZ-based sBCs, increasing the proportion of QZ introduces a greater number of surface-bound cationic groups from GTMAC (showed in the ζ-potential data), leading to stronger electrostatic repulsion between particles. This repulsion reduces interparticle attraction and prevents coalescence, resulting in smaller and more uniform particles, especially at higher QZ content (*e.g.*, QZ100). However, increasing the fraction of unmodified zein, which is inherently hydrophobic in nature due to its high content of non-polar amino acids, leads to strong hydrophobic interactions and reduced solubility in aqueous media. During LLPS, these hydrophobic domains of the zein protein promote uncontrolled aggregation and particle fusion, resulting in larger and more polydisperse condensates, and the effect is particularly evident in QZ30. The diameter of sBCs composed of PEG-conjugated zein (PZ) mixed with the unmodified protein, are presented in Fig. 4B. We also observed that the sBCs exhibited a gradual reduction in particle size with a decreasing amount of zein in the composition. Theoretically, PEG molecules tend to shield the hydrophobic regions of the protein and stabilize the sBCs by reducing surface interactions and promoting steric hindrance between the particles and biomolecules.[80] When the weight fraction of PZ increases in individual sBCs, there would be more effective steric stabilization, preventing particle growth, Ostwald ripening, and maintenance of smaller D_H. Condensates composed of PZ and unmodified zein also promoted tighter packing of particle-constituting biomolecules, most likely due to the flexible chains of the PEG.[81] The sBCs condensed solely with PZ (*i.e.* PZ 100 composition) showed the lowest D_H of 70 ± 7 nm with a PDI of 0.05. On the other hand, PZ70 sBCs, *i.e.* those composed of mixing 70% w/w PZ with 30% w/w of unmodified zein, exhibited a larger D_H of 127 ± 9 nm with a PDI of 0.1. The sBCs composed of lower w/w% of PZ, as in PZ 50 or PZ 30 compositions exhibited larger D_H of 502 ± 34 nm and 342 ± 115 nm, respectively with heterogeneous particle distribution (PDI > 0.5). In the case of PZ sBCs the steric barrier minimizes van der Waals and hydrophobic attractions between particles, restricting growth and aggregation during LLPS. As the PZ content increases, the D_H decreases due to enhanced steric stabilization, with PZ100 showing the smallest diameter. The hydrophobic interactions of unmodified zein in PZ30 and PZ50 systems, on the other hand, increase the D_H. Therefore, the observed size variation across different compositions reflects a dynamic balance between hydrophobic interactions from unmodified zein and stabilizing forces introduced by either quaternization *via* GTMAC (electrostatic) or PEGylation (steric).

3.9. Surface charge distribution is critical for sBC stability

The electrostatic repulsion or attraction between colloidal particles such as those in sBCs is determined by the surface

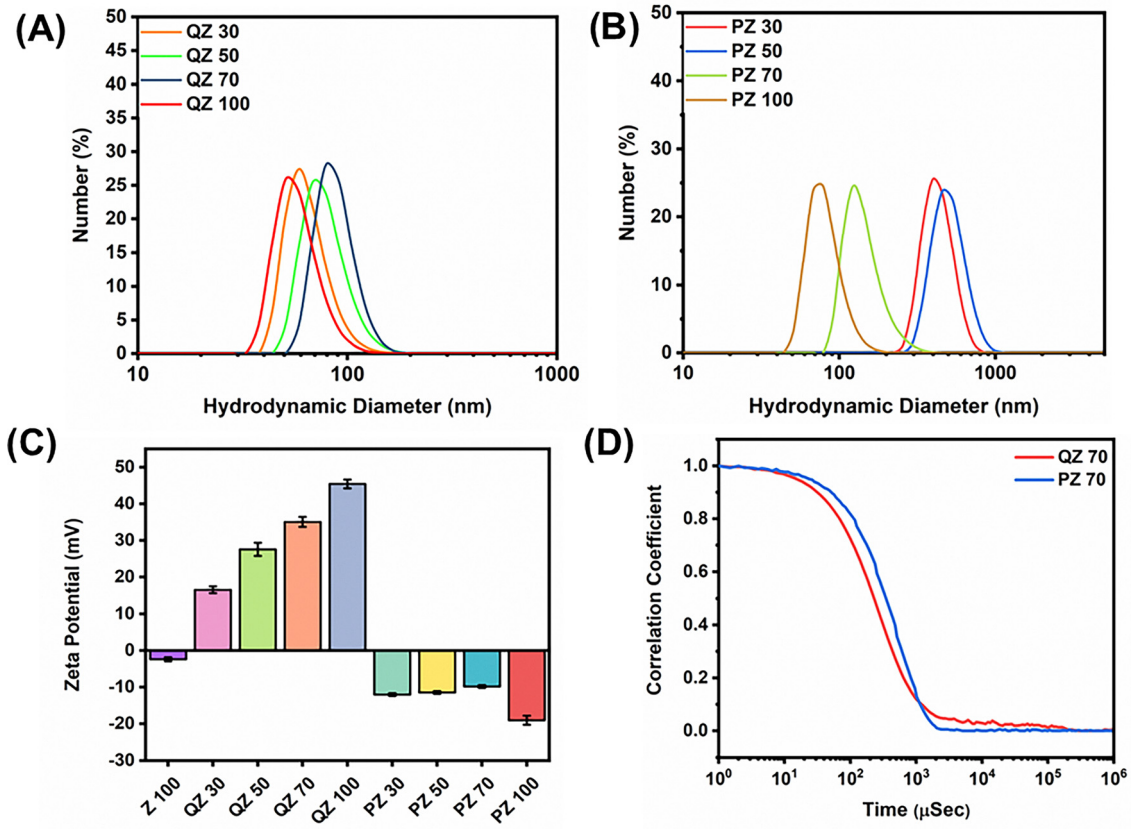

Fig. 4 Size and surface charge characterization of different compositions of sBCs prepared from modified zein: (A) D_H of sBCs formed *via* mixing of zein with QZ at different w/w%; (B) D_H of sBCs formed *via* mixing zein with PZ at different w/w%; (C) ζ-Potential of sBCs formed from zein and QZ or PZ at different w/w% ratio; (D) autocorrelation function of sBCs composed of zein mixed with 70% w/w modified zein (QZ or PZ).

charge, which can be assessed through zeta (ζ-) potential measurements. Typically, particles with a high ζ-potential offer both kinetic and electrostatic stability, helping to prevent particle aggregation in colloidal systems.[82] The ζ-potential of $>+25$ mV or <-25 mV is generally considered ideal for ensuring good colloidal stability as it predicts strong electrostatic repulsive forces between colloidal particles.[83] The zein condensates exhibit an inherent negative surface charge of -2.39 ± 0.5 mV most likely due to the existence of glutamate residues within the primary structure of the protein.[84,85] This reduced zeta potential might be responsible for the higher aggregation tendency of sBCs which are exclusively composed of zein. We evaluated the ζ-potential of the sBCs composed of zein mixed with PZ or QZ to understand the compositional effect on the surface electronic properties of sBCs. As shown in Fig. 4C, there is a gradual increase in the ζ-potential of sBCs with increasing concentration of QZ within the composition. For example, the incorporation of 30% w/w QZ in sBCs increased the ζ-potential up to 16.5 ± 1 mV, while the inclusion of 70% w/w of QZ enhanced the potential up to 35 ± 1 mV. Such significant enhancement in surface charge will favor the formation of stable sBCs not prone to colloidal aggregation due to electrostatic repulsion.

The surface potentials of the sBCs mixed with PZ vary significantly depending on the PEG concentration. For example, the ζ-potential of PZ 30 sBCs, composed of 30% w/w of PZ and 70% w/w of unmodified zein demonstrated a ζ-potential of -12 ± 1 mV. At higher PEG concentrations, the surface charge became markedly negative, as seen in PZ 100 sBCs (-19 ± 1 mV), as shown in Fig. 4C. In these sBCs, which are composed of PEG-conjugated, and unmodified zein, the interactions between the PEG chains on the sBC surfaces most likely caused a partial shielding of the charges.[86] Therefore, we observe that the zeta potential of PZ100 particles appears to be the highest compared with that of PZ70 sBCs (-19.0 mV compared to -9.8 mV). Similarly, PZ 30, PZ 50 and PZ 70 sBCs also exhibited a similar range of zeta potentials (-9.8 to -12.0 mV). This significant increase in the magnitude of negative ζ-potential for PZ enriched sBCs can be attributed to the anionic nature of PEG,[80] which contributes to the electrosteric repulsion between sBCs, potentially providing augmented colloidal stability.[87] Time-dependent evolution of sBC particle size was evaluated using the autocorrelation function during the light scattering experiment by analyzing the fluctuations in scattered light intensity over time (Fig. 4D). Usually, a faster decay in the autocorrelation function indicates smaller particles, and the decay rate of this function is directly related to the particle size and diffusion coefficient of the sBCs in the solution. We observed that for sBCs, the decay rate was faster for QZ or

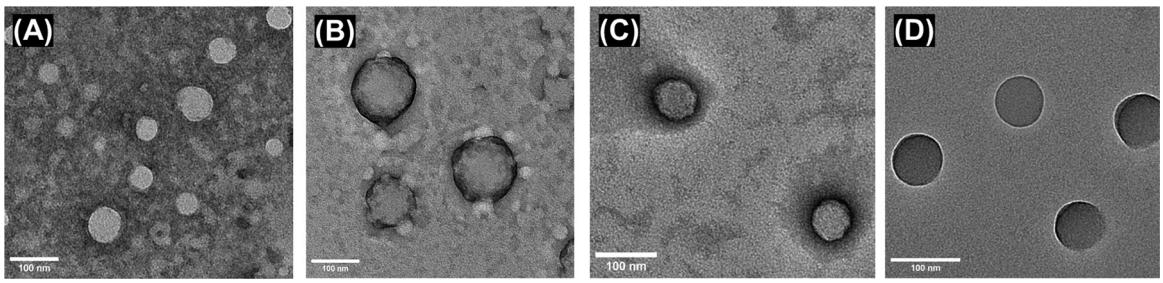

Fig. 5 HR-TEM images of the sBCs of different compositions: (A) QZ100, composed exclusively of quaternized zein protein; (B) QZ70, composed of 70% w/w QZ mixed with 30% w/w unmodified zein; (C) PZ100, composed of PZ and showing a homogeneous representation of spherical particles with uniform size distribution, and (D) PZ70, composed of 70% w/w of PZ mixed with 30% w/w unmodified zein.

PZ containing condensates, compared to those formed from zein only. This observation indicates that compositional variation affects the stability and compaction of sBCs. The autocorrelation function of all compositions of sBCs (both of QZ and PZ variants) are shown in Fig. S2(A and B) (ESI†). The direct imaging of sBCs of different compositions *via* TEM clearly presents the colloidal condensates of the biomolecules, not bound by any membrane-type architecture (Fig. 5A–D). The structures of sBCs, irrespective of their composition, appear to be compact, spherical, and uniformly distributed. All compositions of sBCs, composed of either QZ or PZs, preserved the spherical, particulate morphology as presented in Fig. S3(A–D) (ESI†).

3.10. Evaluation of surface and mechanical characteristics of sBCs by AFM

The morphological and biomechanical properties of sBCs were examined using atomic force microscopy (AFM). Our findings revealed a spherical shape for both sBCs, with PZ70 exhibiting a slightly greater height compared to QZ70, as shown in Fig. 6A and B. These results align well with the size measurements obtained from DLS and TEM analyses (Fig. 4 and 5). Surface stiffness was assessed by analyzing force-dependent distances on the sBC surfaces (Fig. 6C). The mean stiffness values for PZ70 and QZ70 were 139.9 ± 49.22 MPa and 325.4 ± 68.05 MPa, respectively, indicating that PZ70 is over two times softer than QZ70. This is most likely due to the presence of a flexible and dynamic PEG chain on PZ70 surfaces. On the other hand, the surface roughness measurement of sBCs revealed that PZ70 has a less smooth surface compared to QZ70 (Fig. 6D). This is most likely due to the surface presentation of the protein domains which are hydrophilic, most likely composed of residues rich in short GTMAC moieties. Thus, the single-particle nanomechanical analysis suggests that the shape, flexibility, size, and surface smoothness of the sBCs are dependent on the chemical nature (MW and charge) of the residues added to the constituent biomolecules.

3.11. Evaluation of the thermodynamic stability of sBCs

The thermodynamic stability of sBCs is the key to their independent existence. Therefore, the extent of the stability of sBCs was analyzed using the pyrene-based fluorescent spectroscopic assay that is widely used for determining the association stability of condensates composed of amphiphilic macromolecules. The minimum concentration of biomolecules which is required to form an assembly/condensate is known as the critical association concentration (CAC). We selected QZ70 and PZ70 as our representative sBCs to determine the CAC of the biomolecules that are required to form sBCs. Pyrene is used as a fluorescence probe for determining CAC. Typically, the first (λ_{373}) and third ($\lambda_{384\,nm}$) peaks in the fluorescence emission spectra of pyrene are sensitive to the environmental polarity, and the intensity ratio I_{373}/I_{384} serves as an indicator of the aggregation behavior of amphiphilic molecules.[88] Fig. 7A and B

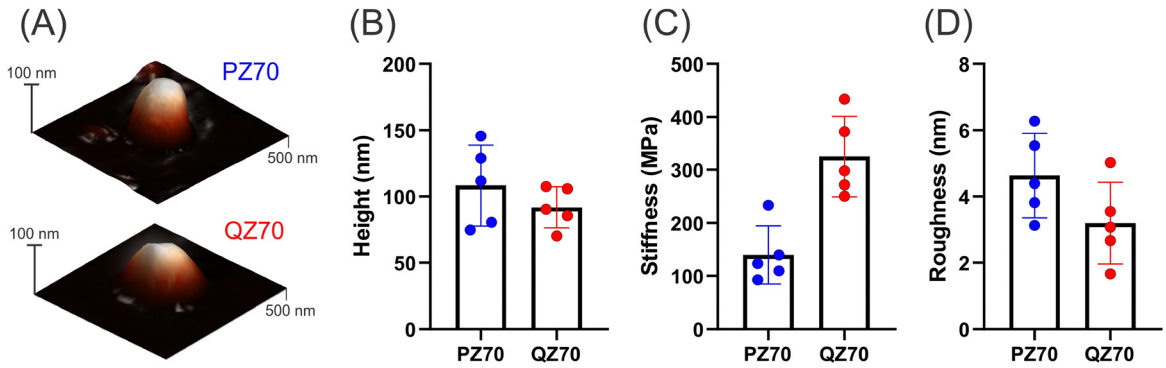

Fig. 6 AFM analysis of sBCs. (A) Topographic images of single PZ70 and QZ70 samples. Comparisons of their (B) heights, (C) stiffness, and (D) surface roughness.

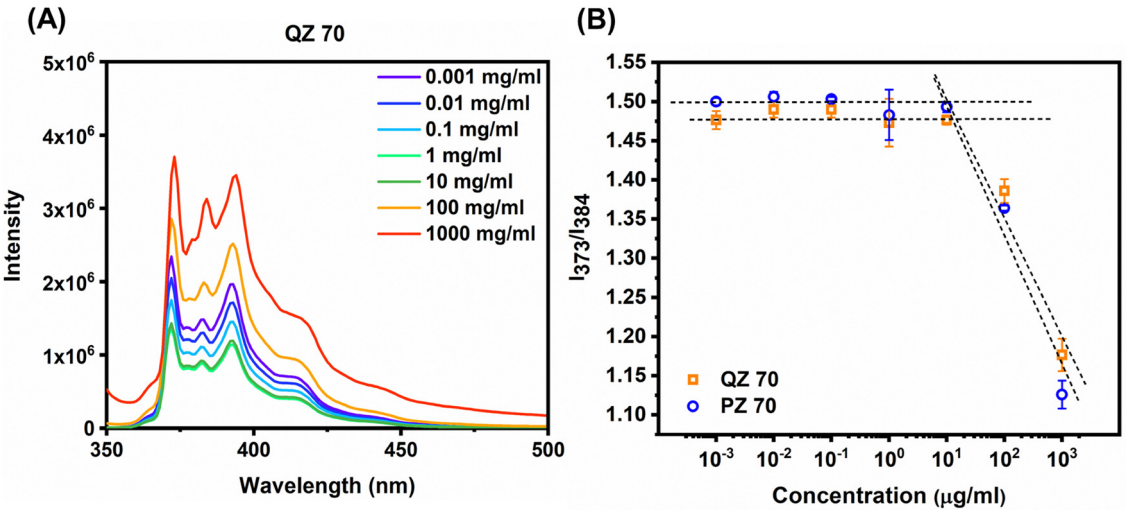

Fig. 7 Thermodynamic stability determined *via* pyrene based critical aggregation concentration assay: (A) intensity *vs.* wavelength spectra for QZ 70 sBCs; (B) I_{373}/I_{384} *vs.* concentration graph showing the CAC of both QZ 70 and PZ 70 at ~10 μg mL^{-1}.

show the effect of sBCs' microenvironment on pyrene fluorescence. The spectral change of pyrene fluorescence in the presence of QZ70 sBCs is presented in Fig. 7A, while for that for PZ70 sBCs is presented in Fig. S4 (ESI†). The ratio of I_{373}/I_{384} was determined from this spectrum and plotted as a function of sBC concentration (Fig. 7B). From Fig. 7B, we observe that at lower concentrations (below 1 μg mL^{-1}), both QZ70 and PZ70 sBCs exhibit a high I_{373}/I_{384} ratio of ~1.5, indicating that the molecules are well-dispersed as a discrete entity within a polar environment of sBCs. No significant aggregation has occurred in this region. As the concentration increases from 10^{-3} to 10 μg mL^{-1}, the I_{373}/I_{384} ratio remains relatively stable, suggesting that the protein molecules maintain a dispersed state up until this range. From a 10 μg mL^{-1} concentration onwards, a sharp decrease in the I_{373}/I_{384} ratio is observed for both QZ70 and PZ70 sBCs as shown in Fig. 7B. This indicates that the system is reaching the CAC, where the local environment around pyrene becomes less polar due to the formation of aggregates, and pyrene becomes partitioned into the hydrophobic core of these sBCs. This results in a marked decrease in the I_{373}/I_{384} ratio, indicating a transition from a polar to a hydrophobic environment. Beyond a 10 μg mL^{-1} concentration of protein, there is a significant reduction in the I_{373}/I_{384} ratio, which can be observed for both formulations. This experiment reveals that zein mixed with QZ or PZ form sBCs at a relatively low CAC (~10 μg mL^{-1}), suggesting that the sBCs can form and remain stable even at low concentrations.[89,90]

3.12. Capacity of sBCs to compartmentalize a guest molecule

To evaluate the capacity of the sBCs composed of zein and modified zein to compartmentalize a small molecular weight guest molecule, we used doxorubicin (DOX). This compound is selected because of its hydrophilicity, pH-dependent solubility, and ease of quantification by UV-Vis or fluorescence spectrophotometry. We first determined the loading efficiency, *i.e.*, how much quantity of the added small molecular compound can be accumulated within the condensate using eqn (2) presented in Section 2.16. Afterward, we evaluated the fraction of the compound that can be encapsulated or compartmentalized in a specific weight fraction of the condensate-forming macromolecules using eqn (3) (Section 2.16). The amount of the loading efficiency and the loading content is presented in Table 2.

Table 2 Loading efficiency and content of DOX condensed within sBCs

sBC-composition	Loading efficiency	Loading content
QZ70	19.3 ± 0.08	2.89 ± 0.01
PZ70	27.6 ± 1	4.14 ± 018

Interestingly, we observe that sBC composition did not affect the loading efficiency or the content significantly. This is most likely due to the pK_a of DOX (pK_a = 8.3), which is mostly contributed by the primary amine functional group present in the sugar residue of DOX. Under preparative conditions, a larger mole fraction of the drug remained protonated, which favored electrostatic interactions with sBC components. We also evaluated the kinetics at which the DOX is dissociated from the sBCs. We selected QZ 70 and PZ 70 sBCs to evaluate the DOX dissociation kinetics from sBCs under different pH conditions, *i.e.* at pH 7.4 and 5.5. Fig. 8B displays the cumulative dissociation profile of DOX from sBCs composed of QZ mixed with the modified protein at a 70% w/w ratio. The DOX cumulative release profile for PZ 70 sBCs is shown in Fig. S5 (ESI†). For QZ 70 systems the cumulative dissociation of DOX gradually increases and reaches a plateau at around ~3.5% for the pH 5.5 system and ~2% for the pH 7.4 system at the end of 33 h. Overall the extent of DOX dissociation from sBCs such as QZ70 is slightly higher at pH 5.5 than that at pH 7.4 (Fig. 8B). This dissociation experiment showed that the small molecules, such as DOX, can be compartmentalized within the sBCs, mostly facilitated by electrostatic interactions. At relatively

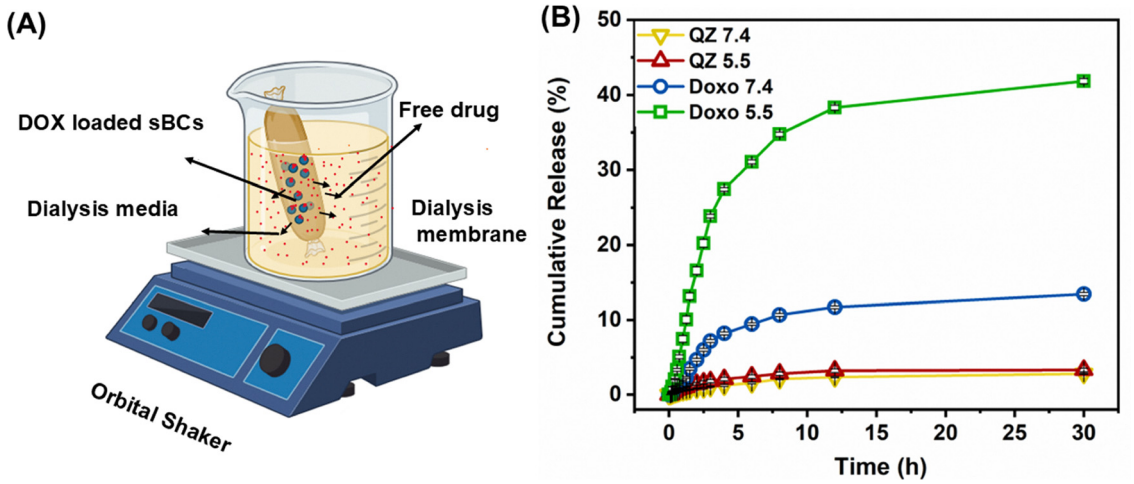

Fig. 8 Cumulative dissociation of DOX from the sBCs: (A) experimental setup for DOX dissociation from the sBCs over time; (B) dissociation of DOX from QZ70 sBCs as a function of time under two different pH conditions.

acidic pH, the primary amine group of DOX is ionized, which may have contributed to the slightly faster rate of DOX dissociation from sBCs. For PZ 70 sBCs, the dissociation of DOX from sBCs is more suppressed compared to that observed from QZ systems, indicating higher compartmentalization of the small molecule within the condensed particles (Fig. S5, ESI†).

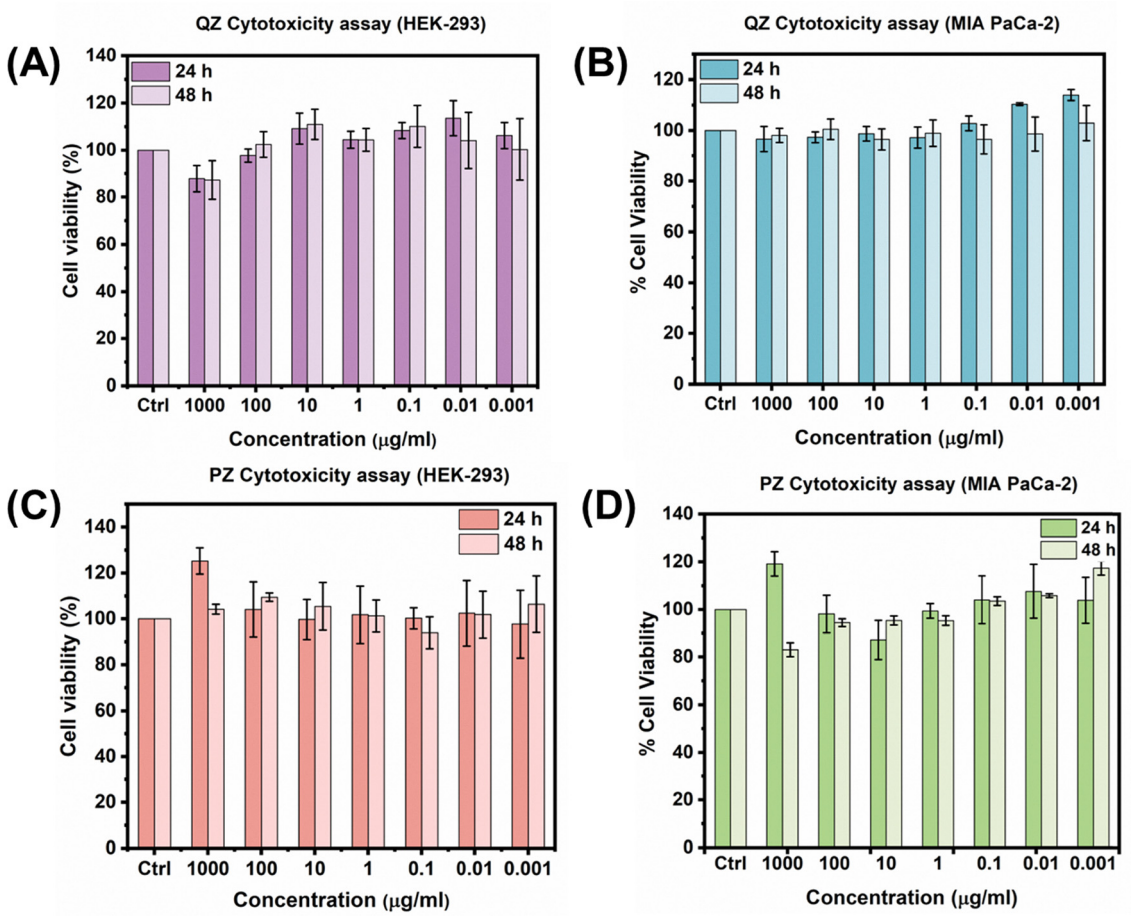

Fig. 9 Effect of sBCs containing QZ or PZ mixed with zein on MIA-PaCa-2 and HEK-293 cell lines for 24–48 h: (A) cytotoxic effects of QZ70 on HEK-293 cell lines; (B) cytotoxic effects of QZ70 on MIA PaCa-2 cell lines; (C) cytotoxic effects of PZ70 on HEK-293 cell lines; (D) PZ70 cytotoxic effects on MIA PaCa-2 cell lines.

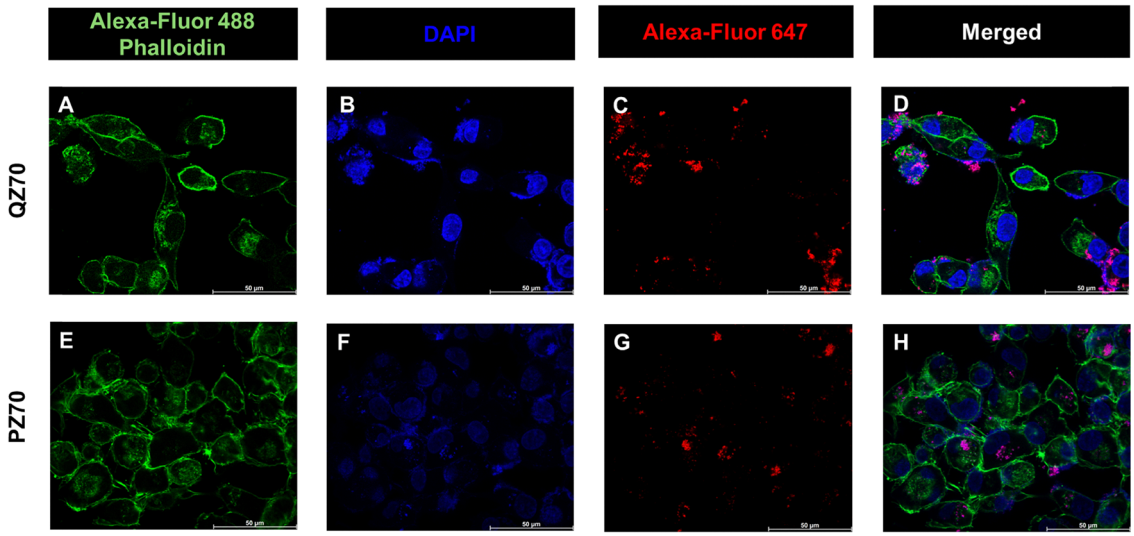

Fig. 10 Confocal fluorescence microscopic images showing sBC distribution *in vitro* (10 mg, 24 h). Top panel: (A)–(D) the confocal microscopy images of cellular uptake of Alexa fluor 647 tagged QZ70 sBCs (Red). Bottom panel: (E)–(H) the confocal microscopy images of cellular uptake of Alexa fluor 647 tagged synthetic condensates (Red).

DOX itself is a weakly basic compound with a pK_a value of 8.01 and becomes more soluble at lower pH due to protonation.[91,92] This increased hydrophilicity of DOX coupled with the tortuous, PEG-rich surface of PZ sBCs are most likely responsible for the slight suppression of the rate and extent of DOX dissociation from the PZ sBCs. As a control experiment, we added the same concentration of free DOX inside the dialysis membrane and repeated the same method. From Fig. 8B, we observe that at pH 7.4, DOX shows a cumulative release of 13% over 30 h, while at pH 5.5, a significantly higher cumulative release of 42% was observed, indicating that sBCs can compartmentalize DOX extensively from the bulk environment.

3.13. Cellular effect of sBCs

We evaluated the cellular effect of sBCs composed of QZ or PZ mixed with unmodified zein using the Alamar blue assay in two different cell lines: human embryonic kidney (HEK293) and MIA PaCa-2 pancreatic cancer cells. We selected the sBCs composed of 70% w/w of QZ or PZ proteins mixed with zein because these condensates showed uniform particle size distribution ranging from 130–150 nm, and surface properties ranging from +28 mV to −17 mV conducive for potential *in vitro* or *in vivo* studies. The cells were incubated with varying concentrations (1000–0.001 μg mL^{-1}) of these sBCs for 24 or 48 h to evaluate their impact on cells. The cytotoxicity data is presented in Fig. 9A–D. Our experiment revealed that both QZ and PZ containing sBC compositions did not exert any significant cytotoxicity across the range of tested concentrations. The cell viability remained >90% for both formulations in both cell lines over 24–48 h.

3.14. Cellular internalization and uptake of sBCs

We evaluated the cellular internalization of sBCs composed of zein and PZ or QZ. For labeling zein with a fluorescent dye, we conjugated Alexa Fluor 647 NHS ester to the N-terminal residue of the protein *via* an EDC/NHS mediated amide coupling reaction. Confocal laser scanning microscopy was used to determine the cellular uptake of QZ70 and PZ70 particles in MIA PaCa-2 cell lines. These systems presented either a cationized or a PEG-enriched surface, respectively. We observed that QZ 70 systems show an enhanced affinity towards cell membranes compared to PZ-rich sBCs (Fig. 10). This is most likely due to the presence of a positively charged surface on QZ70 sBCs, which promoted non-specific cellular uptake of the particles through the cell membrane. On the other hand, PZ70 sBCs exhibited relatively higher cellular internalization compared to QZ70 particles.

4. Conclusion

In this study, we developed an approach to engineer synthetic biomolecular condensates (sBCs) from a plant protein. Mimicking the natural processes of condensate formation, we mixed proteins of diversified chemical motifs, which were precipitated as colloidally stable entities *via* LLPS. The primary structure of the protein was modified *via* quaternization and PEG conjugation, copying the natural mechanism of post-translational modifications. The sBCs were found to form spherical particles with controllable colloidal properties such as size, surface charge, and stability. In most cases, the sizes and charges were found to be a function of the composition of sBCs. As such, this work can open pathways to provide a straightforward strategy to engineer artificial biomolecular condensates with compartmentalization functions for small molecules or reaction partners. The approach can be used to produce synthetic cells and cellular organelles, where condensates of pre-programmed stability and function are required for efficient biomolecular communications.

Conflicts of interest

The authors declare no conflicts of interest.

Data availability

The data that support the findings of the study are available from the corresponding author M. Q. upon reasonable request.

Acknowledgements

This research was supported by NSF CBET 2239629 (to M. Q.), and partially supported by the National Science Foundation under NSF EPSCoR Track-1 Cooperative Agreement OIA #1946202 (MQ), and NIH grant no. 2P20 GM109024 from the National Institute of General Medicine (NIGMS, to MQ as senior personnel), and NSF CBET 2317111 (to Y. C.). Its contents are solely the responsibility of the authors and do not necessarily represent the official views of the NIH. Any opinions, findings, conclusions, or recommendations expressed are those of the authors and do not necessarily reflect the views of the National Science Foundation. The authors would like to thank Scott Payne and Jayma Moore for the TEM imaging. We would like to acknowledge the core confocal microscopy facility Department of Pharmaceutical Science NDSU supported under the Dakota Cancer Collaboration on translational activity (DaCCoTA CTR) (NIH/NIGMS: U54GM128729).

References

1 S. F. Banani, H. O. Lee, A. A. Hyman and M. K. Rosen, Biomolecular condensates: organizers of cellular biochemistry, *Nat. Rev. Mol. Cell Biol.*, 2017, **18**(5), 285–298, DOI: **10.1038/nrm.2017.7**.

2 S. Boeynaems, S. Alberti, N. L. Fawzi, T. Mittag, M. Polymenidou, F. Rousseau, J. Schymkowitz, J. Shorter, B. Wolozin and L. Van Den Bosch, *et al.*, Protein Phase Separation: A New Phase in Cell Biology, *Trends Cell Biol.*, 2018, **28**(6), 420–435, DOI: **10.1016/j.tcb.2018.02.004**.

3 A. S. Lyon, W. B. Peeples and M. K. Rosen, A framework for understanding the functions of biomolecular condensates across scales, *Nat. Rev. Mol. Cell Biol.*, 2021, **22**(3), 215–235, DOI: **10.1038/s41580-020-00303-z**.

4 S. Alberti and D. Dormann, Liquid-Liquid Phase Separation in Disease, *Annu. Rev. Genet.*, 2019, **53**, 171–194, DOI: **10.1146/annurev-genet-112618-043527**.

5 S. Elbaum-Garfinkle, Matter over mind: Liquid phase separation and neurodegeneration, *J. Biol. Chem.*, 2019, **294**(18), 7160–7168, DOI: **10.1074/jbc.REV118.001188**.

6 S. Alberti and A. A. Hyman, Are aberrant phase transitions a driver of cellular aging, *Bioessays*, 2016, **38**(10), 959–968, DOI: **10.1002/bies.201600042**.

7 A. Boija, I. A. Klein and R. A. Young, Biomolecular Condensates and Cancer, *Cancer Cell*, 2021, **39**(2), 174–192, DOI: **10.1016/j.ccell.2020.12.003**.

8 A. Abyzov, M. Blackledge and M. Zweckstetter, Conformational Dynamics of Intrinsically Disordered Proteins Regulate Biomolecular Condensate Chemistry, *Chem. Rev.*, 2022, **122**(6), 6719–6748, DOI: **10.1021/acs.chemrev.1c00774**.

9 Y. Dai, L. You and A. Chilkoti, Engineering synthetic biomolecular condensates, *Nat. Rev. Bioeng.*, 2023, 1–15, DOI: **10.1038/s44222-023-00052-6**.

10 R. L. Hastings and S. Boeynaems, Designer Condensates: A Toolkit for the Biomolecular Architect, *J. Mol. Biol.*, 2021, **433**(12), 166837, DOI: **10.1016/j.jmb.2021.166837**.

11 E. Corradini, P. S. Curti, A. B. Meniqueti, A. F. Martins, A. F. Rubira and E. C. Muniz, Recent Advances in Food-Packing, Pharmaceutical and Biomedical Applications of Zein and Zein-Based Materials, *Int. J. Mol. Sci.*, 2014, **15**(12), 22438–22470.

12 F. Dong, X. Dong, L. Zhou, H. Xiao, P.-Y. Ho, M.-S. Wong and Y. Wang, Doxorubicin-loaded biodegradable self-assembly zein nanoparticle and its anti-cancer effect: Preparation, in vitro evaluation, and cellular uptake, *Colloids Surf., B*, 2016, **140**, 324–331, DOI: **10.1016/j.colsurfb.2015.12.048**.

13 C. J. Cheng, M. Ferruzzi and O. G. Jones, Fate of lutein-containing zein nanoparticles following simulated gastric and intestinal digestion, *Food Hydrocolloids*, 2019, **87**, 229–236, DOI: **10.1016/j.foodhyd.2018.08.013**.

14 L. Wang, J. Xue and Y. Zhang, Preparation and characterization of curcumin loaded caseinate/zein nanocomposite film using pH-driven method, *Ind. Crops Prod.*, 2019, **130**, 71–80, DOI: **10.1016/j.indcrop.2018.12.072**.

15 S. Podaralla and O. Perumal, Preparation of Zein Nanoparticles by pH Controlled Nanoprecipitation, *J. Biomed. Nanotechnol.*, 2010, **6**(4), 312–317, DOI: **10.1166/jbn.2010.1137**.

16 X. Yan, M. Li, X. Xu, X. Liu and F. Liu, Zein-based nanodelivery systems for encapsulation and protection of hydrophobic bioactives: A review, *Front. Nutr.*, 2022, **9**, 999373, DOI: **10.3389/fnut.2022.999373**.

17 H. T. Phan and A. J. Haes, What Does Nanoparticle Stability Mean?, *J. Phys. Chem. C*, 2019, **123**(27), 16495–16507.

18 R. Shukla and M. Cheryan, Zein: the industrial protein from corn, *Ind. Crops Prod.*, 2001, **13**(3), 171–192, DOI: **10.1016/S0926-6690(00)00064-9**.

19 D. Segets, R. Marczak, S. Schäfer, C. Paula, J.-F. Gnichwitz, A. Hirsch and W. Peukert, Experimental and theoretical studies of the colloidal stability of nanoparticles-a general interpretation based on stability maps, *ACS Nano*, 2011, **5**(6), 4658–4669.

20 Y. V. Kuznetsova, I. A. Balyakin, I. D. Popov, B. Schummer, B. Sochor, S. V. Rempel and A. A. Rempel, Ag2S interparticle interaction in an aqueous solution: Mechanism of steric and electrostatic stabilization, *J. Mol. Liq.*, 2021, **335**, 116130, DOI: **10.1016/j.molliq.2021.116130**.

21 S. Hirsjärvi, L. J. Peltonen and J. Hirvonen, Surface pressure measurements in particle interaction and stability studies of poly(lactic acid) nanoparticles, *Int. J. Pharm.*, 2008, **348**(1–2), 153–160.

22 W. Ryoo, J. L. Dickson, V. V. Dhanuka, S. E. Webber, R. T. Bonnecaze and K. P. Johnston, Electrostatic Stabilization of Colloids in Carbon Dioxide: Electrophoresis and Dielectrophoresis, *Langmuir*, 2005, **21**(13), 5914–5923, DOI: **10.1021/la046770w**.

23 S. V. N. T. Kuchibhatla, A. S. Karakoti and S. Seal, Colloidal stability by surface modification, *JOM*, 2005, **57**(12), 52–56, DOI: **10.1007/s11837-005-0183-1**.

24 L. Xu, H. Liang, Y. Yang and S. Yu, Stability and Reactivity: Positive and Negative Aspects for Nanoparticle Processing, *Chem. Rev.*, 2018, **118**(7), 3209–3250.

25 B. Chanteau, J. Fresnais and J. F. Berret, Electrosteric enhanced stability of functional sub-10 nm cerium and iron oxide particles in cell culture medium, *Langmuir*, 2009, **25**(16), 9064–9070.

26 W.-C. Luo, A. O'Reilly Beringhs, R. Kim, W. Zhang, S. M. Patel, R. H. Bogner and X. Lu, Impact of formulation on the quality and stability of freeze-dried nanoparticles, *Eur. J. Pharm. Biopharm.*, 2021, **169**, 256–267, DOI: **10.1016/j.ejpb.2021.10.014**.

27 M. K. Lee, M. Y. Kim, S. Kim and J. Lee, Cryoprotectants for freeze drying of drug nano-suspensions: Effect of freezing rate, *J. Pharm. Sci.*, 2009, **98**(12), 4808–4817, DOI: **10.1002/jps.21786**.

28 Y. Zhang, L. Cui, F. Li, N. Shi, C. Li, X. Yu, Y. Chen and W. Kong, Design, fabrication and biomedical applications of zein-based nano/micro-carrier systems, *Int. J. Pharm.*, 2016, **513**(1), 191–210, DOI: **10.1016/j.ijpharm.2016.09.023**.

29 A. R. Patel, E. C. M. Bouwens and K. P. Velikov, Sodium Caseinate Stabilized Zein Colloidal Particles, *J. Agric. Food Chem.*, 2010, **58**(23), 12497–12503, DOI: **10.1021/jf102959b**.

30 G. Davidov-Pardo, I. J. Joye and D. J. McClements, Encapsulation of resveratrol in biopolymer particles produced using liquid antisolvent precipitation. Part 1: Preparation and characterization, *Food Hydrocolloids*, 2015, **45**, 309–316, DOI: **10.1016/j.foodhyd.2014.11.023**.

31 Y. Luo, T. T. Y. Wang, Z. Teng, P. Chen, J. Sun and Q. Wang, Encapsulation of indole-3-carbinol and 3,3′-diindolylmethane in zein/carboxymethyl chitosan nanoparticles with controlled release property and improved stability, *Food Chem.*, 2013, **139**(1), 224–230, DOI: **10.1016/j.foodchem.2013.01.113**.

32 J. Chen, J. Zheng, D. J. McClements and H. Xiao, Tangeretin-loaded protein nanoparticles fabricated from zein/β-lactoglobulin: Preparation, characterization, and functional performance, *Food Chem.*, 2014, **158**, 466–472, DOI: **10.1016/j.foodchem.2014.03.003**.

33 D. S. Silva, W. M. Facchinatto, D. M. dos Santos, F. I. Boni, T. A. Valdes, A. Leitão, M. P. D. Gremião, L. A. Colnago, S. P. Campana-Filho and S. J. L. Ribeiro, N-(2-hydroxy)-propyl-3-trimethylammonium, O-palmitoyl chitosan: Synthesis, physicochemical and biological properties, *Int. J. Biol. Macromol.*, 2021, **178**, 558–568, DOI: **10.1016/j.ijbiomac.2021.02.031**.

34 N. C. Sarker, P. Ray, C. Pfau, V. Kalavacharla, K. Hossain and M. Quadir, Development of Functional Nanomaterials from Wheat Bran Derived Arabinoxylan for Nucleic Acid Delivery, *J. Agric. Food Chem.*, 2020, **68**(15), 4367–4373, DOI: **10.1021/acs.jafc.0c00029**.

35 Z. Liu, Y. Ni, P. Fatehi and A. Saeed, Isolation and cationization of hemicelluloses from pre-hydrolysis liquor of kraft-based dissolving pulp production process, *Biomass Bioenergy*, 2011, **35**(5), 1789–1796, DOI: **10.1016/j.biombioe.2011.01.008**.

36 S. Alexey, Catalytic Reductive Amination of Aldehydes and Ketones With Nitro Compounds: New Light on an Old Reaction, *Front. Chem.*, 2020, **8**, 215, DOI: **10.3389/fchem.2020.00215**.

37 E. M. Dangerfield, C. H. Plunkett, A. L. Win-Mason, B. L. Stocker and M. S. Timmer, Protecting-Group-Free Synthesis of Amines: Synthesis of Primary Amines from Aldehydes via Reductive Amination, *J. Org. Chem.*, 2010, **75**(16), 5470–5477, DOI: **10.1021/jo100004c**.

38 M. Friedman, Applications of the Ninhydrin Reaction for Analysis of Amino Acids, Peptides, and Proteins to Agricultural and Biomedical Sciences, *J. Agric. Food Chem.*, 2004, **52**(3), 385–406, DOI: **10.1021/jf030490p**.

39 M. R. H. Khan, Z. Armstrong, M. Lenertz, B. Saenz, N. Kale, Q. Li, A. MacRae, Z. Yang and M. Quadir, Metal–Organic Framework Induced Stabilization of Proteins in Polymeric Nanoparticles, *ACS Appl. Mater. Interfaces*, 2024, **16**(12), 14405–14420, DOI: **10.1021/acsami.3c16534**.

40 W. S. Saad and R. K. Prud'homme, Principles of nanoparticle formation by flash nanoprecipitation, *Nano Today*, 2016, **11**(2), 212–227, DOI: **10.1016/j.nantod.2016.04.006**.

41 R. S. Hazra, J. Roy, L. Jiang, D. C. Webster, M. M. Rahman and M. Quadir, Biobased, Macro-, and Nanoscale Fungicide Delivery Approaches for Plant Fungi Control, *ACS Applied Bio Mater.*, 2023, 2576–6422.

42 L. Alhalhooly, M. I. Confeld, S. O. Woo, B. Mamnoon, R. Jacobson, S. Ghosh, J. Kim, S. Mallik and Y. Choi, Single-Molecule Force Probing of RGD-Binding Integrins on Pancreatic Cancer Cells, *ACS Appl. Mater. Interfaces*, 2022, **14**(6), 7671–7679, DOI: **10.1021/acsami.1c23361**.

43 V. Natarajan, S. Ha, A. Delgado, R. Jacobson, L. Alhalhooly, Y. Choi and J. Kim, Acquired αSMA Expression in Pericytes Coincides with Aberrant Vascular Structure and Function in Pancreatic Ductal Adenocarcinoma, *Cancers*, 2022, **14**(10), 2448, DOI: **10.3390/cancers14102448**.

44 L. Alhalhooly, B. Mamnoon, J. Kim, S. Mallik and Y. Choi, Dynamic cellular biomechanics in responses to chemotherapeutic drug in hypoxia probed by atomic force spectroscopy, *Oncotarget*, 2021, **12**(12), 1165–1177, DOI: **10.18632/oncotarget.27974**.

45 K. Bansal, D. Webster and M. Quadir, Self-Assembled Nanostructures from Amphiphilic Sucrose-Soyates for Solubilizing Hydrophobic Guest Molecules, *Langmuir*, 2022, **38**(6), 2066–2075, DOI: **10.1021/acs.langmuir.1c03033**.

46 A. I. Elegbede, J. Banerjee, A. J. Hanson, S. Tobwala, B. Ganguli, R. Wang, X. Lu, D. K. Srivastava and S. Mallik, Mechanistic Studies of the Triggered Release of Liposomal Contents by Matrix Metalloproteinase-9, *J. Am. Chem. Soc.*, 2008, **130**(32), 10633–10642, DOI: **10.1021/ja801548g**.

47 Y. Z. Zhao, C. Z. Sun, C. T. Lu, D. D. Dai, H. F. Lv, Y. Wu, C. W. Wan, L. J. Chen, M. Lin and X. K. Li, Characterization and anti-tumor activity of chemical conjugation of doxorubicin in polymeric micelles (DOX-P) in vitro, *Cancer Lett.*, 2011, **311**(2), 187–194, DOI: 10.1016/j.canlet.2011.07.013.

48 L. E. Scheeren, D. R. Nogueira-Librelotto, J. R. Fernandes, L. B. Macedo, A. I. Marcolino, M. P. Vinardell and C. M. Rolim, Comparative Study of Reversed-Phase High-Performance Liquid Chromatography and Ultraviolet-Visible Spectrophotometry to Determine Doxorubicin in pH-Sensitive Nanoparticles, *Anal. Lett.*, 2018, **51**(10), 1445–1463, DOI: 10.1080/00032719.2017.1380034.

49 R. S. Hazra, D. Dutta, B. Mamnoon, G. Nair, A. Knight, S. Mallik, S. Ganai, K. Reindl, L. Jiang and M. Quadir, Polymeric Composite Matrix with High Biobased Content as Pharmaceutically Relevant Molecular Encapsulation and Release Platform, *ACS Appl. Mater. Interfaces*, 2021, **13**(34), 40229–40248, DOI: 10.1021/acsami.1c03805.

50 K. Salaita, P. M. Nair, R. S. Petit, R. M. Neve, D. Das, J. W. Gray and J. T. Groves, Restriction of receptor movement alters cellular response: physical force sensing by EphA2, *Science*, 2010, **327**(5971), 1380–1385, DOI: 10.1126/science.1181729.

51 M. Sugimoto, A. Inoko, T. Shiromizu, M. Nakayama, P. Zou, S. Yonemura, Y. Hayashi, I. Izawa, M. Sasoh and Y. Uji, *et al.*, The keratin-binding protein Albatross regulates polarization of epithelial cells, *J. Cell Biol.*, 2008, **183**(1), 19–28, DOI: 10.1083/jcb.200803133.

52 M. Fallah-Mehrjardi, A. R. Kiasat and K. Niknam, Nucleophilic ring-opening of epoxides: trends in β-substituted alcohols synthesis, *J. Iran. Chem. Soc.*, 2018, **15**(9), 2033–2081, DOI: 10.1007/s13738-018-1400-5.

53 C. Reboredo, C. J. González-Navarro, A. L. Martínez-López and J. M. Irache, Oral administration of zein-based nanoparticles reduces glycemia and improves glucose tolerance in rats, *Int. J. Pharm.*, 2022, **628**, 122255, DOI: 10.1016/j.ijpharm.2022.122255.

54 H. A. Wiggers, M. T. Fin, N. M. Khalil and R. M. Mainardes, Polyethylene Glycol-Stabilized Zein Nanoparticles Containing Gallic Acid, *Food Technol. Biotechnol.*, 2022, **60**(2), 145–154, DOI: 10.17113/ftb.60.02.22.6981.

55 P. Satheesh, A. Ranjith, A. Mohammed and P. Omathanu, Synthesis of Novel Biodegradable Methoxy Poly(ethylene glycol)–Zein Micelles for Effective Delivery of Curcumin, *Mol. Pharm.*, 2012, (9), 2778, DOI: 10.1021/mp2006455.

56 Z. C. Soe, W. Ou, M. Gautam, K. Poudel, B. K. Kim, L. M. Pham, C. D. Phung, J.-H. Jeong, S. G. Jin and H.-G. Choi, *et al.*, Development of Folate-Functionalized PEGylated Zein Nanoparticles for Ligand-Directed Delivery of Paclitaxel, *Pharmaceutics*, 2019, **11**, 562.

57 J. E. Habben, A. W. Kirleis and B. A. Larkins, The origin of lysine-containing proteins in opaque-2 maize endosperm, *Plant Mol. Biol.*, 1993, **23**(4), 825–838, DOI: 10.1007/BF00021537.

58 G. Chand, V. Muthusamy, R. U. Zunjare, S. J. Mishra, G. Sharma, B. K. Mehta, S. Singh, T. Allen and F. Hossain, Molecular analysis of opaque2 gene governing accumulation of lysine and tryptophan in maize endosperm, *Euphytica*, 2024, **220**(10), 155, DOI: 10.1007/s10681-024-03414-2.

59 S. S. Hong, R. K. Thapa, J. H. Kim, S. Y. Kim, J. O. Kim, J. K. Kim, H. G. Choi and S. J. Lim, Role of zein incorporation on hydrophobic drug-loading capacity and colloidal stability of phospholipid nanoparticles, *Colloids Surf., B*, 2018, **171**, 514–521, DOI: 10.1016/j.colsurfb.2018.07.068.

60 H. Liang, Q. Huang, B. Zhou, L. He, L. Lin, Y. An, Y. Li, S. Liu, Y. Chen and B. Li, Self-assembled zein–sodium carboxymethyl cellulose nanoparticles as an effective drug carrier and transporter, *J. Mater. Chem. B*, 2015, **3**(16), 3242–3253, DOI: 10.1039/C4TB01920B.

61 F. Dai, Q. Zhuang, G. Huang, H. Deng and X. Zhang, Infrared Spectrum Characteristics and Quantification of OH Groups in Coal, *ACS Omega*, 2023, **8**(19), 17064–17076, DOI: 10.1021/acsomega.3c01336.

62 T. Noguchi, Y. Inoue and X. S. Tang, Structure of a Histidine Ligand in the Photosynthetic Oxygen-Evolving Complex As Studied by Light-Induced Fourier Transform Infrared Difference Spectroscopy, *Biochemistry*, 1999, **38**(31), 10187–10195, DOI: 10.1021/bi990631.

63 H. Hu, M. Yu, F. Li, Z. Chen, X. Gao, L. Xiong and C. Huang, Facile Epoxidation Strategy for Producing Amphiphilic Up-Converting Rare-Earth Nanophosphors as Biological Labels, *Chem. Mater.*, 2008, **20**(22), 7003–7009, DOI: 10.1021/cm801215t.

64 F. Mendel, Solvent effects in the absorption spectra of the Ninhydrin chromophore, *Microchem. J.*, 1971, **16**(2), 204–209, DOI: 10.1016/0026-265X(71)90110-X.

65 D. P. Erickson, O. K. Ozturk, G. Selling, F. Chen, O. H. Campanella and B. R. Hamaker, Corn zein undergoes conformational changes to higher β-sheet content during its self-assembly in an increasingly hydrophilic solvent, *Int. J. Biol. Macromol.*, 2020, **157**, 232–239, DOI: 10.1016/j.ijbiomac.2020.04.169.

66 S. M. Kelly, T. J. Jess and N. C. Price, How to study proteins by circular dichroism, *Biochim. Biophys. Acta, Proteins Proteomics*, 2005, **1751**(2), 119–139, DOI: 10.1016/j.bbapap.2005.06.005.

67 V. Cabra, R. Arreguin, A. Galvez, M. Quirasco, R. Vazquez-Duhalt and A. Farres, Characterization of a 19 kDa α-Zein of High Purity, *J. Agric. Food Chem.*, 2005, **53**(3), 725–729, DOI: 10.1021/jf048530s.

68 G. W. Selling, S. A. Hamaker and D. J. Sessa, Effect of Solvent and Temperature on Secondary and Tertiary Structure of Zein by Circular Dichroism, *Cereal Chem.*, 2007, **84**(3), 265–270, DOI: 10.1094/CCHEM-84-3-0265.

69 L. Qu, G. Chen, S. Dong, Y. Huo, Z. Yin, S. Li and Y. Chen, Improved mechanical and antimicrobial properties of zein/chitosan films by adding highly dispersed nano-TiO2, *Ind. Crops Prod.*, 2019, **130**, 450–458, DOI: 10.1016/j.indcrop.2018.12.093.

70 M. A. Moreno, M. E. Orqueda, L. G. Gómez-Mascaraque, M. I. Isla and A. López-Rubio, Crosslinked electrospun zein-based food packaging coatings containing bioactive chilto

fruit extracts, *Food Hydrocolloids*, 2019, **95**, 496–505, DOI: 10.1016/j.foodhyd.2019.05.001.

71 H. Wu, C. Tong, C. Wu and J. Pang, Production and characterization of composite films with zein nanoparticles based on the complexity of continuous film matrix, *LWT*, 2022, **161**, 113396, DOI: 10.1016/j.lwt.2022.113396.

72 F. M. Veronese and A. Mero, The Impact of PEGylation on Biological Therapies, *BioDrugs*, 2008, **22**(5), 315–329, DOI: 10.2165/00063030-200822050-00004.

73 S. S. Devangamath, B. Lobo, S. P. Masti and S. Narasagoudr, Thermal, mechanical, and AC electrical studies of PVA–PEG–Ag_2S polymer hybrid material, *J. Mater. Sci.: Mater. Electron.*, 2020, **31**(4), 2904–2917, DOI: 10.1007/s10854-019-02835-3.

74 B. T. DiTullio, C. J. Wright, P. Hayes, P. J. Molino and T. W. Hanks, Surface modification of polyaniline nanorods with thiol-terminated poly(ethylene oxide, *Colloid Polym. Sci.*, 2018, **296**(4), 637–645, DOI: 10.1007/s00396-018-4278-y.

75 P. Fatehi and H. Xiao, Adsorption Characteristics of Cationic-Modified Poly (Vinyl Alcohol) on Cellulose Fibers–A Qualitative Analysis, *Colloids Surf., A*, 2008, **327**(1–3), 127.

76 A. M. Sajjan, B. K. Jeevan Kumar, A. A. Kittur and M. Y. Kariduraganavar, Development of novel grafted hybrid PVA membranes using glycidyltrimethylammonium chloride for pervaporation separation of water–isopropanol mixtures, *J. Ind. Eng. Chem.*, 2013, **19**(2), 427–437, DOI: 10.1016/j.jiec.2012.08.032.

77 T. J. Anderson and B. P. Lamsal, Zein extraction from corn, corn products, and coproducts and modifications for various applications: a review, *Cereal Chem.*, 2011, **88**(2), 159–173.

78 Q. Zhong and M. Jin, Zein nanoparticles produced by liquid–liquid dispersion, *Food Hydrocolloids*, 2009, **23**(8), 2380–2387, DOI: 10.1016/j.foodhyd.2009.06.015.

79 Y. Song, J. Zhou, Q. Li, Y. Guo and L. Zhang, Preparation and Characterization of Novel Quaternized Cellulose Nanoparticles as Protein Carriers, *Macromol. Biosci.*, 2009, **9**(9), 857–863, DOI: 10.1002/mabi.200800371.

80 C. Reboredo, C. J. González-Navarro, C. Martínez-Oharriz, A. L. Martínez-López and J. M. Irache, Preparation and evaluation of PEG-coated zein nanoparticles for oral drug delivery purposes, *Int. J. Pharm.*, 2021, **597**, 120287, DOI: 10.1016/j.ijpharm.2021.120287.

81 J. Lin, H. Zhang, V. Morovati and R. Dargazany, PEGylation on mixed monolayer gold nanoparticles: Effect of grafting density, chain length, and surface curvature, *J. Colloid Interface Sci.*, 2017, **504**, 325–333, DOI: 10.1016/j.jcis.2017.05.046.

82 K. Y. Win and S. S. Feng, Effects of particle size and surface coating on cellular uptake of polymeric nanoparticles for oral delivery of anticancer drugs, *Biomaterials*, 2005, **26**(15), 2713–2722, DOI: 10.1016/j.biomaterials.2004.07.050.

83 S. Mahobia, J. Bajpai and A. K. Bajpai, An *In-vitro* Investigation of Swelling Controlled Delivery of Insulin from Egg Albumin Nanocarriers, *Iran. J. Pharm. Res.*, 2016, **15**(4), 1735-0328.

84 D. Qin, L. Zhang, X. Du, Y. Wang and Q. Zhang, Simple and green synthesis of protein-conjugated CdS nanoparticles and spectroscopic study on the interaction between CdS and zein, *J. Nanopart. Res.*, 2016, **18**(9), 254, DOI: 10.1007/s11051-016-3568-x.

85 H. Yin, T. Lu, L. Liu and C. Lu, Preparation, characterization and application of a novel biodegradable macromolecule: Carboxymethyl zein, *Int. J. Biol. Macromol.*, 2015, **72**, 480–486, DOI: 10.1016/j.ijbiomac.2014.08.025.

86 N. T. Thi Nguyen, S. Yun, D. W. Lim and E. K. Lee, Shielding effect of a PEG molecule of a mono-PEGylated peptide varies with PEG chain length, *Prep. Biochem. Biotechnol.*, 2018, **48**(6), 522–527, DOI: 10.1080/10826068.2018.1466157.

87 X. Zhang, M. R. Servos and J. Liu, Ultrahigh Nanoparticle Stability against Salt, pH, and Solvent with Retained Surface Accessibility via Depletion Stabilization, *J. Am. Chem. Soc.*, 2012, **134**(24), 9910–9913, DOI: 10.1021/ja303787e.

88 P. Ray, N. Kale and M. Quadir, New side chain design for pH-responsive block copolymers for drug delivery, *Colloids Surf., B*, 2021, **200**, 111563, DOI: 10.1016/j.colsurfb.2021.111563.

89 X. Yang, Q. Zhang, Y. Wang, H. Chen, H. Zhang, F. Gao and L. Liu, Self-aggregated nanoparticles from methoxy poly(ethylene glycol)-modified chitosan: Synthesis; characterization; aggregation and methotrexate release in vitro, *Colloids Surf., B*, 2008, **61**(2), 125–131, DOI: 10.1016/j.colsurfb.2007.07.012.

90 J. M. Yu, Y. J. Li, L. Y. Qiu and Y. Jin, Self-aggregated nanoparticles of cholesterol-modified glycol chitosan conjugate: Preparation, characterization, and preliminary assessment as a new drug delivery carrier, *Eur. Polym. J.*, 2008, **44**(3), 555–565, DOI: 10.1016/j.eurpolymj.2008.01.013.

91 C. Du, D. Deng, L. Shan, S. Wan, J. Cao, J. Tian, S. Achilefu and Y. Gu, A pH-sensitive doxorubicin prodrug based on folate-conjugated BSA for tumor-targeted drug delivery, *Biomaterials*, 2013, **34**, 3087–3097.

92 M. Mahdavi, F. Rahmani and S. Nouranian, Molecular simulation of pH-dependent diffusion, loading, and release of doxorubicin in graphene and graphene oxide drug delivery systems, *J. Mater. Chem. B*, 2016, **4**(46), 7441–7451, DOI: 10.1039/C6TB00746E.